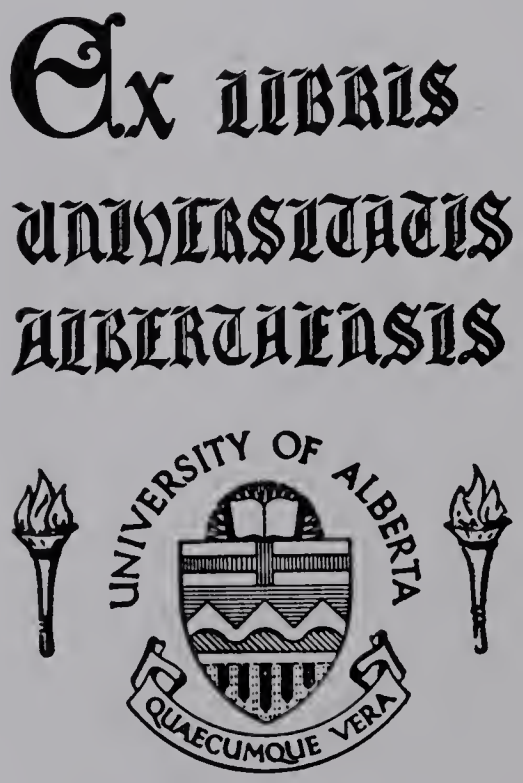

University of Alberta
Printing Department

THE UNIVERSITY OF ALBERTA

THE $C^{12}(D,N)N^{13}$ REACTION AT 6 MEV

by

Andrew Wesley Obst

A THESIS

SUBMITTED TO THE FACULTY OF GRADUATE STUDIES

IN PARTIAL FULFILMENT OF THE REQUIREMENTS FOR THE DEGREE

OF MASTER OF SCIENCE

DEPARTMENT OF PHYSICS

EDMONTON, ALBERTA

August, 1966

UNIVERSITY OF ALBERTA

FACULTY OF GRADUATE STUDIES

The undersigned certify that they have read, and recommend to the Faculty of Graduate Studies for acceptance, a thesis entitled THE $C^{12}(D,N)N^{13}$ REACTION AT 6 MEV, submitted by Andrew Wesley Obst in partial fulfilment of the requirements for the degree of Master of Science.

ABSTRACT

The $C^{12}(d,n)N^{13}$ reaction has been studied at a deuteron bombarding energy of 6 MeV. Angular distributions of the neutrons leading to the ground, 2.367 and the unresolved 3.51-3.56 MeV states were obtained.

The ground ($J^\pi = 1/2^-$), 2.367 ($J^\pi = 1/2^+$) and the unseparated 3.56 ($J^\pi = 5/2^+$) MeV states were analyzed with the plane wave Born approximation. An analysis of the separated 3.51 ($J^\pi = 3/2^-$) and 3.56 MeV states was attempted. The ground state was analyzed using the distorted wave Born approximation.

Spectroscopic factors were extracted for the four levels of N^{13}. The width of the unseparated doublet in N^{13} at 3.51-3.56 MeV was found to be about 71 keV. There was no evidence of spin dependent structure for this nucleus at this energy.

An appendix describes the conversion of two elastic search codes along with an outline of the theory relevant to (d,n) reactions.

ACKNOWLEDGEMENTS

I would like to thank my supervisors; Dr. W.K. Dawson for suggestions on points of analysis, and Dr. G. Roy both for initiating the project and for providing and maintaining much enthusiasm over the past year.

Particular thanks are due to Dr. G.C. Neilson for suggesting the project and for his constant participation in its execution. Providing an excellent spectrometer and making the experiment possible is only part of his contribution.

Special thanks are due to Dr. W.J. MacDonald and Mr. D.A. Gedcke for the smooth operation of the spectrometer, as well as many points on analysis.

The assistance of Mr. T.B. Grandy is gratefully acknowledged.

Finally I would like to thank Mrs. L. Medford for her meticulous effort in typing the manuscript and the University of Alberta for providing financial support for the duration of this work.

TABLE OF CONTENTS

FIGURES

FIGURES (Continued)

I. INTRODUCTION

a. Motivation for the Experiment

Nuclear stripping reactions (Gl 63) have provided physicists with an extremely useful tool for studying the properties of nuclei. This is due to the fact that only a few nucleons are actively involved in the reaction, as well as the fact that bound nuclear states can be reached. From physical considerations it is apparent that the cross section will involve the overlap of wave functions describing the initial system with those describing the final system. Because of the few degrees of freedom involved such an overlap measures the degree to which the passive nucleons occupy the same configuration in the initial and final states.

Furthermore the fact that there are only three active particles involved enables an unambiguous determination to be made of the angular momentum of the captured particle. Conservation of angular momentum imposes a restriction on the spin state of the final nucleus. Explicitly we must satisfy

$$\underline{J}_i + \underline{\ell}_p + 1/2 = \underline{J}_f, \quad \pi_i \pi_f = (-1)^{\ell_p} \qquad \text{(I-1)}$$

for a (d,n) reaction. $\underline{\ell}_p$ is the angular momentum of the captured proton, and $\underline{J}_i$, π_i and $\underline{J}_f$, π_f are the spins and parities of the initial and final

nuclei respectively.

The angular distribution of the emitted neutron is frequently characteristic of the value of $\underline{\ell}_p$, and if $\underline{J}_i$ is known this allows close limits to be set on $\underline{J}_f$. At best, when the target nucleus has zero spin, the final spin is limited to $J_f = \ell \pm 1/2$. The remaining ambiguity can only be resolved by polarization or γ-ray correlation experiments.

Lee and Schiffer (Le 64) have recently observed for (d,p) reactions a consistent difference in the structure of angular distributions of states populated by the same ℓ-value neutrons but differing in J_f. The effect was most evident for $\ell_n = 1$. For these transitions and deuteron energies between 7 and 12 MeV, $40 < A < 65$, and spectroscopic factors greater than about 0.1 (see section IV d) the $J_f = 1/2$ states exhibit a sharp minimum somewhere in the range $90° < \theta < 145°$ but $J_f = 3/2$ states do not. The effect decreases with decrease in energy. Experiments with light nuclei do not seem to show this trend.

The purpose of this experiment was then to investigate the presence of this effect in light nuclei, in particular with the $C^{12}(d,n)$ reaction to the ground state, $J^\pi = 1/2^-$, and to the second excited state, $J^\pi = 3/2^-$. It was necessary to split the doublet in N^{13} at 3.51 - 3.56 MeV excitation in order to extract the minor component (Figure 1-1). A bombarding energy of 6 MeV provided optimum spectrometer resolution. The procedure and success of resolving the doublet is described in section III b. The existence of an excellent

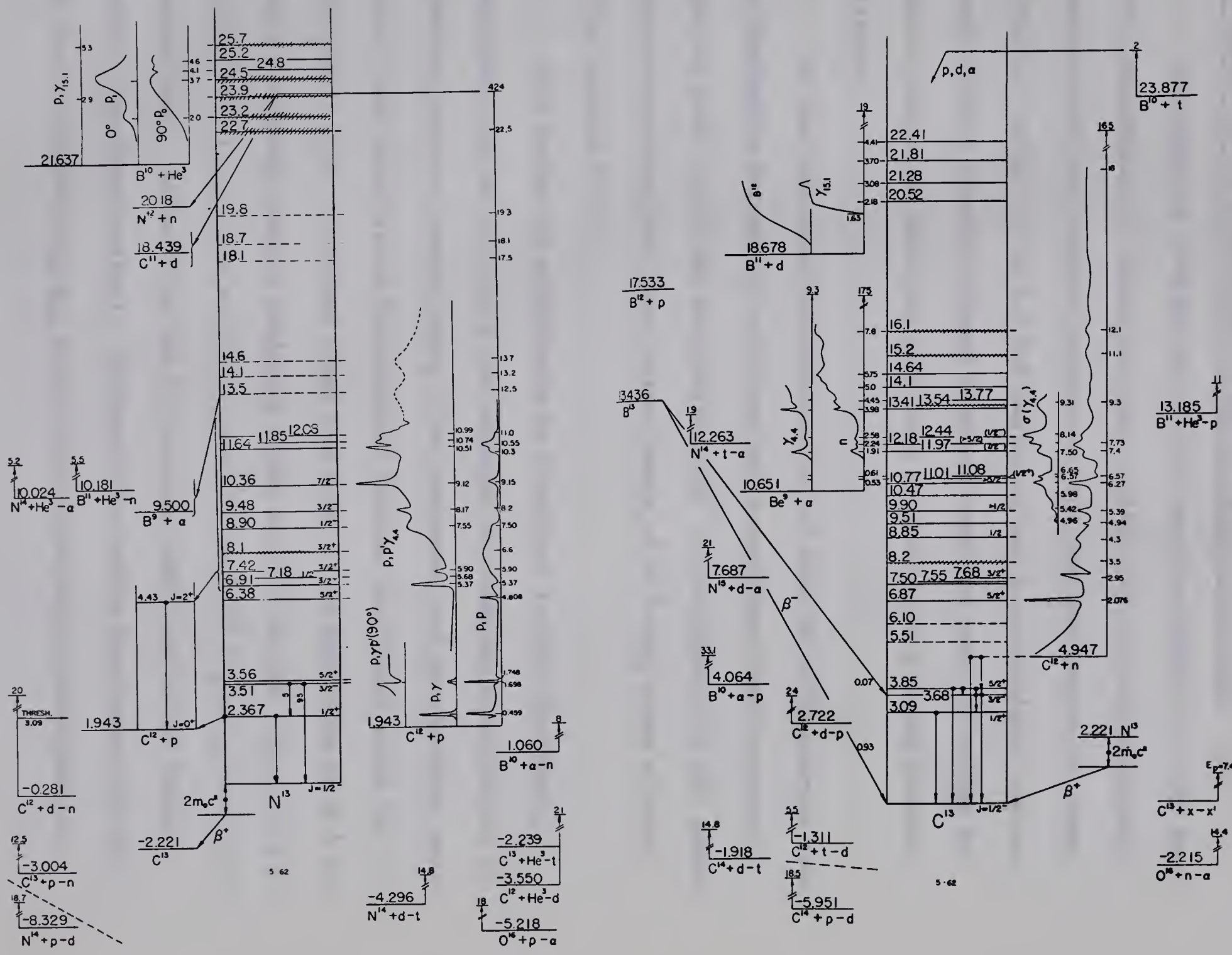

FIGURE 1-1. ENERGY LEVELS OF THE MIRROR NUCLEI C^{13} - N^{13}

fast neutron time-of-flight spectrometer made this work at all possible.

b. Survey of the Literature on the $C^{12}(d,n)N^{13}$ Reaction

Beginning in 1940 and up to 1951 reaction products of the deuteron bombardment of carbon had been studied (Bo 49), and analysed assuming that the compound nucleus was the dominant source of these products. Using 0.7 to 1.9 MeV deuterons and a proportional counter, Bonner (ibid.) however already observed that the ratio of proton to neutron yields was much too high when compared with Coulomb penetrabilities.

In the same year Grosskreutz (Gr 49) with 10 MeV deuterons from the Washington University cyclotron and photoplates first reported a state at 3.48 ± 0.12 MeV excitation in N^{13}. Van Patter (Va 49) subsequently associated the first three levels of N^{13} with those of the mirror nucleus C^{13}.

In a series of experiments at Liverpool in 1951 El-Bedewi, Middleton, and Tai (El 51) first reported the angular distribution of separated neutron groups, using 8 MeV deuterons and photographic emulsions. They interpreted the neutrons feeding the ground state (Q = -0.24 MeV), 2.38 ± 0.05 MeV state and 3.53 ± 0.05 MeV state of N^{13} by Newn's stripping theory, assigning spins of $3/2^-$ or $1/2^-$ ($\ell_p = 1$, R = 5.5 f), $1/2^+$ ($\ell_p = 0$, R = 6.3 f), and $5/2^+$ or $3/2^+$ ($\ell_p = 2$, R = 6.3 f), respectively. Butler fits (Mi 53) yielded radii one to two fermis smaller (the Gamow radius). However for a radius consistent for all the states Middleton et al. found that Butler theory predicted the

wrong ℓ-value for the first excited state. They therefore concluded that for this particular Q-value and their deuteron energy Butler theory is incorrect; probably due to the singular behaviour near the binding energy of the deuteron. They found other discrepancies common to this experiment. These were an experimental forward minimum which is not predicted for $\ell_p = 1$ and the forward maximum for the 3.53 MeV group where ℓ_p is not zero, which is characteristic of high negative Q values. If one allows some arbitrariness in the radius then ℓ is not uniquely determined in this latter case. Comparison with the mirror nucleus C^{13} and the shell model confirmed the $P_{1/2}$ and $S_{1/2}$ nature of the ground and first excited states, respectively. Concerning the second excited state, Jackson and Galonsky (Ja 51) first reported it as a doublet from elastic proton scattering, consisting of a $P_{3/2}$ state at 3.503 MeV and a $D_{5/2}$ state at 3.550 MeV. Rotblat (Ro 51) confirmed two similar states in C^{13} at 3.683 and 3.884 MeV with spins $P_{1/2}$ or $P_{3/2}$ and $D_{3/2}$ or $D_{5/2}$, respectively.

Wilkinson (Wi 55) made use of the unique property of N^{13} that its excited states are all unbound to proton emission to measure total $C^{12}(d,n)N^{13}$ cross sections to the ground state. He passed a 20 MeV deuteron beam through polyethylene foils stacked between sheets of aluminum. The residual β^+ activity plotted against time and extrapolated back to when the beam was stopped yielded the total cross section. He found a smooth excitation function. This suggested little compound nucleus formation, although at the higher energies the

aluminum foils represented some 500 kilovolts thickness. The observed total cross section was 100 mb at E_d = 8 MeV.

Bonner et al. (Bo 56) studied the (d,n) and (d,p) reactions from C^{12} at 1.8 to 6.1 MeV bombarding energy in an effort to extract the direct, compound, and interference contribution in this transition region. The deuteron source was the 6 MeV Rice Institute Van de Graaff. The proton detector was a scintillation counter while the neutron detector was both a long counter and an energy-sensitive detector made up of four spherical anthracene scintillators. With a 155 $\mu g/cm^2$ target the cross section at E_d = 3.64 MeV for the ground state neutron group was found to be 14 mb/sterad at 30°. Resonances were found at deuteron energies of 2.47, 2.67, 2.99, 3.39, 4.00, 4.6. 4.8, 5.34, and 5.64 MeV. Bonner found, by comparison with Butler theory and by comparing total with first excited state excitation functions, that the neutron (proton) group feeding the first excited state of $N^{13}(C^{13})$ do so more by stripping than those feeding the ground state. Bonner points out, however, that this may be unique for the deuteron energy used , if in the stripping picture one assumes that the disintegration particle has about the same velocity as the incident deuteron. By writing the cross section as a coherent sum of a direct (background) contribution plus a resonant compound nucleus contribution and separated in phase, Bonner found that for the (d,p) reaction at 4 MeV and 30°, the direct contribution was 63%. Of the remaining 37%, 33% was interference and 4% was due to the resonant term alone. In this way

he found angular distributions symmetric about 90° and extracted spins of N^{14*} consistent with other work.

Benenson et al. (Be 55) made a comparison of the differential cross sections for the reactions $C^{12}(d,p)C^{12}$ and $C^{12}(d,n)N^{13}$ at bombarding energies of 2.68 MeV and 3.26 MeV. Using solid and gas targets and a gas recoil neutron spectrometer they obtained absolute cross sections and fitted these to Butler theory. For the (d,p) reaction they first subtracted an isotropic background. In view of the large possible interference this was not a good idea. In contrast with the findings of Middleton et al. (Mi 53), the resulting agreement with Butler theory for the ground state was quite good. They then compared the ratios of the (d,n) cross sections with the ratios of the respective kinetic factors from plane wave stripping theory. They concluded that the reasonable agreement was justified. Of the effects neglected, effects involving the deuteron appear in both reactions. The outgoing proton had an energy over 5 MeV, well above the Coulomb barrier. Furthermore the nuclear scattering phase shifts of the liberated particles, appreciable only for angular momenta less than two, were found to be similar.

Calvert et al. (Ca 57) bombarded carbon with 9 MeV deuterons and found agreement with Butler theory consistent with the work of Middleton et al. (Mi 53), but with a radius parameter of $(1.7 + 1.22A^{1/3})$ fermis, which is the Gamow radius. In addition they measured the absolute cross sections for the three neutron groups, includ-

ing the unresolved doublet.

McEllistrem (Mc 58) made an extensive analysis of the C^{12} + d reaction, showing that the resonances in N^{14*} were of compound nucleus origin. He found corrected reduced widths for the (d,p) reaction by comparing only the higher angular momentum components of an extracted reaction amplitude with that of the Butler amplitude. He concluded that the data could best be represented by a stripping amplitude plus more than one resonant compound nuclear amplitudes.

Elwyn, Kane, Ofer, and Wilkinson (El 59), did the first time-of-flight experiment with $C^{12}(d,n)N^{13}$, at 14 energies from E_d = 1.45 MeV to E_d = 2.95 MeV. They found that the direct reaction was dominant at all the bombarding energies. Fluctuation in the best fit Butler radii were most likely due to the large direct-compound nuclear interference term. They attempted to remove this term by averaging the cross section at the first peak over several deuteron energies. In this way the effects of the excitation energy (equivalently the bombarding energy) sensitive compound state would be eliminated. The resulting fit to Butler theory was quite good in the forward hemisphere. That the compound nuclear contribution itself is small was evidenced in the smoothness of the total integrated cross section. It has been pointed out (Wi 58), in fact, that in low Q stripping with low energy deuterons direct effects should be large on simple physical grounds (see also Gi 61). Consideration of the binding energy of the proton in N^{13}, 1.941 MeV, and the neutron in C^{12}, 18.722 MeV (Ho 61),

led to the conclusion that projectile stripping was the main mechanism. Therefore Coulomb and nuclear effects have to be included to obtain overall agreement.

James (Ja 61) has investigated the $C^{12}(d,n)N^{13}$ reaction below 2 MeV bombarding energy. He found agreement consistent with compound nucleus formation but concluded that charge symmetry in the (d,p) - (d,n) reactions was not conserved because of the presence of an a_4 coefficient in the (d,n) case.

Kolonko *et al.* (Ko 63) bombarded C^{12} with 13 MeV deuterons and analysed the neutrons leading to the ground, first and the unresolved second and third states using Butler theory. Their inconsistent radii were attributed to the singularity in the theory, *i.e.* the state of the final nucleus is an energy state close to the separation energy of the last nucleon (Bh52). They also found that Coulomb corrections to the Butler formula produced a stronger variation of the reduced width with r_o than without this correction.

Jeronymo *et al.* (Je 63) performed the $C^{12}(d,n)C^{13}$ and $C^{12}(d,d)C^{12}$ reactions at bombarding energies from 0.9 to 5 MeV. They found that there is a large resonant contribution in deuteron reactions with C^{12} even at 5 MeV. They point out that since in this nucleus the p subshell is filled, it is possible that due to lack of loosely coupled surface nucleons the incident particle tends to form a compound system. Hence the relative contribution of resonance mechanism compared to direct interactions gets enhanced.

Hodgson (Ho 63) analysed the (d,n) data of Elwyn et al. (El 59) with a zero range distorted wave theory and an arbitrary cut-off radius. He found several sets of optical potential parameters that accounted for the overall distribution. The absolute cross sections however, as in this experiment, were found particularly sensitive to the choice of potentials. Ohlsen and Shamu (Ol 63) have recently scattered 6 MeV deuterons on carbon. Optical potential parameters from their data would no doubt prove useful, though some of the parameters, in particular the absorbing part of the potential, would be more accurately fixed by reaction data. The (d,d) excitation function at 6 MeV lies on the edge of the prominent 15.09 MeV level and on the less prominent 15.44 MeV levels of N^{14*}. This would further affect a direct comparison of elastic with reaction parameters.

Fulbright, Robbins, West, and Saylor (Fu 66) bombarded carbon-12 at energies near the 4 MeV resonance in N^{14*}. They found that at small angles the minimum value of the resonant cross section to the ground state of N^{13} consistent with their analysis is 5 mb/sr. The maximum resonant contribution for the (d,p) case, on the other hand, has been shown by Bonner et al. (Bo 56) to be no greater than 1 mb/sr. While Bonner shows that in the (d,p) case to the ground state of C^{13} the resonant term is small compared to the resonant-direct interference term, Fulbright et al. find that there is little interference in both the (d,n) and (d,p) reactions to the first excited states of N^{13} and C^{13}, respectively, at the same bombarding energy.

The foregoing survey has shown that a proper treatment of the $C^{12}(d,n)N^{13}$ reactions requires a contribution from compound nucleus formation. This is probably due to the closed shell structure of C^{12} and the resulting lack of available single particle states. Conclusions drawn from the present experiment could therefore be invalidated by such unfortuitous interference as studied in the above section, although (d,p) experiments to the ground state of C^{13} at higher energies indicate that this is unlikely.

II. THE EXPERIMENT

a. Experimental Arrangement

The $C^{12}(d,n)N^{13}$ reaction was performed with the University of Alberta 6 MeV model CN [1] Van de Graaff accelerator, utilizing the time-of-flight method with top terminal pulsing and a 75" Mobley compression system (Da 66). The beam transport system is illustrated in Figure 2-1.

Gas is ionized in the source bottle by a 125 mc source oscillator. The stripped electrons are attracted to the positive probe while the positive ions are attracted to an opening called the canal. The helical motion of the electrons is due to the source magnet. This also enhances ionization. Since the net charge in the resulting plasma is zero, the potential between the probe and canal is confined to the Crookes dark space near the canal.

The terminal analysis magnet acts as a mass separator. Focusing is accomplished by a three element electrostatic Einzel lens, the self focusing column, and a quadrupole doublet.

Beam pulsing is achieved by two sets of parallel deflection plates perpendicular to each other. These are driven out of phase by

---

[1]) High Voltage Engineering Corporation, Burlington, Massachusetts, U.S.A.

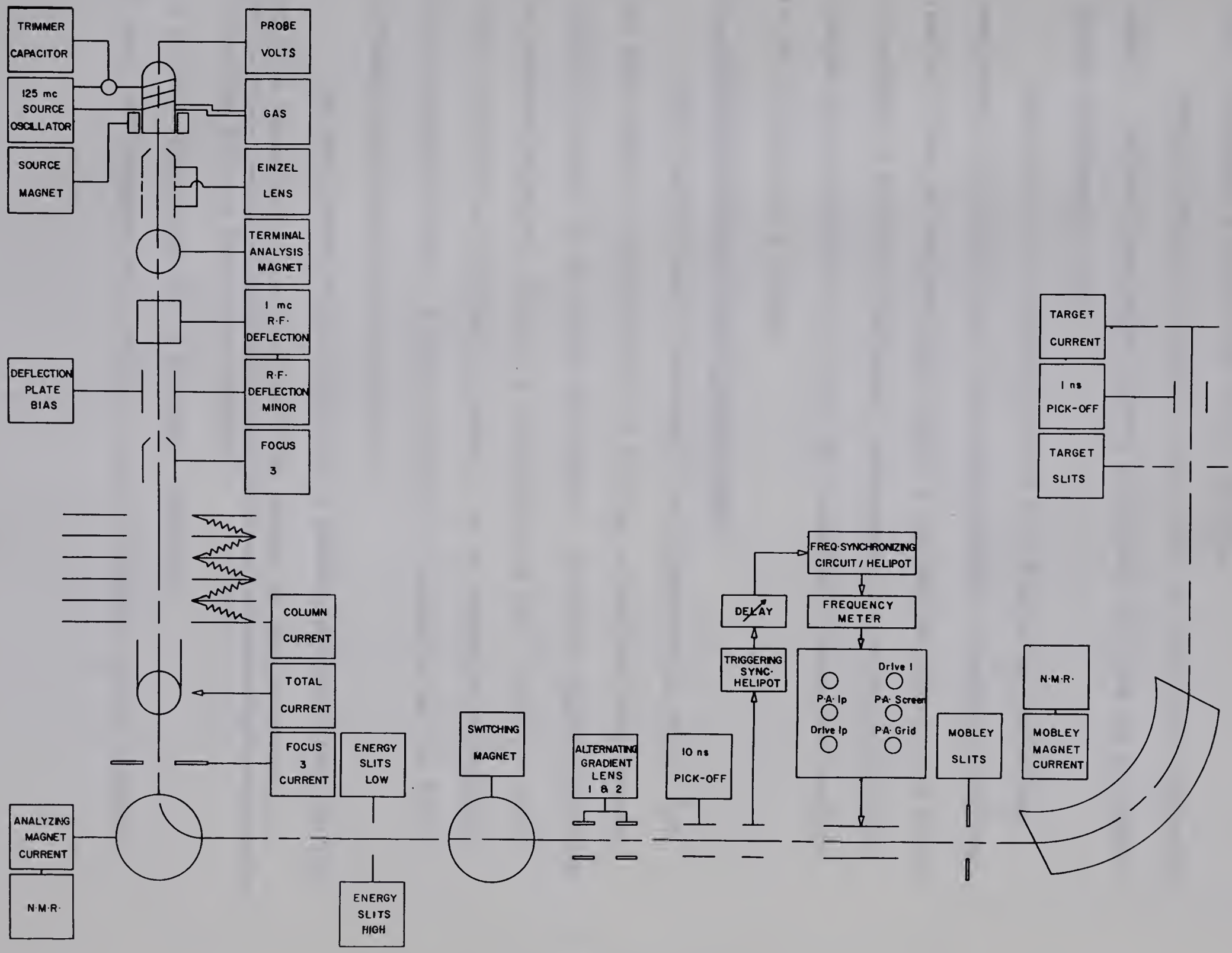

FIGURE 2-1 BLOCK DIAGRAM OF BEAM TRANSPORT SYSTEM

a 1 mc R.F. oscillator. The resulting elliptical motion of the beam over an aperture produces the desired pulsing.

Energy (momentum) analysis of the beam is done by the analyzing magnet. The switching magnet serves to deflect the beam to the appropriate experimental port.

The 10 mc R.F. deflection system [2] deflects the individual beam bursts for compression in the Mobley magnet. Compression is realized by virtue of the same time required for the two ends of the burst to traverse a different distance. The original 10 ns bursts are compressed in this manner to 0.5 ns. The resulting average beam current is of the order of 2 μ amps.

b. The Neutron Time-of-Flight Spectrometer

The time-of-flight spectrometer is illustrated in Figure 2-2. The stop signal is derived from a 3 cm long cylindrical beam sensing capacitor located 30 cm before the target. The start signal comes from the neutron detector. This is a cylindrical Ne 213 [3] 3.45" x 0.75" liquid scintillator enclosed in quartz. It is coupled to a Phillips XP1040 photomultiplier. A Naton phosphor [4] coupled to an RCA 8575 photomultiplier serves as the monitor.

The main detector was mounted on a remote controlled cart at the end of a six meter boom. Neutrons from carbon in the system were

---

[2]) See (Da 66) and references therein.

[3]) Nuclear Enterprises Ltd., Winnipeg, Manitoba.

[4]) Nash and Thompson Ltd., Hookrise South, Tolworth, Surrey, England.

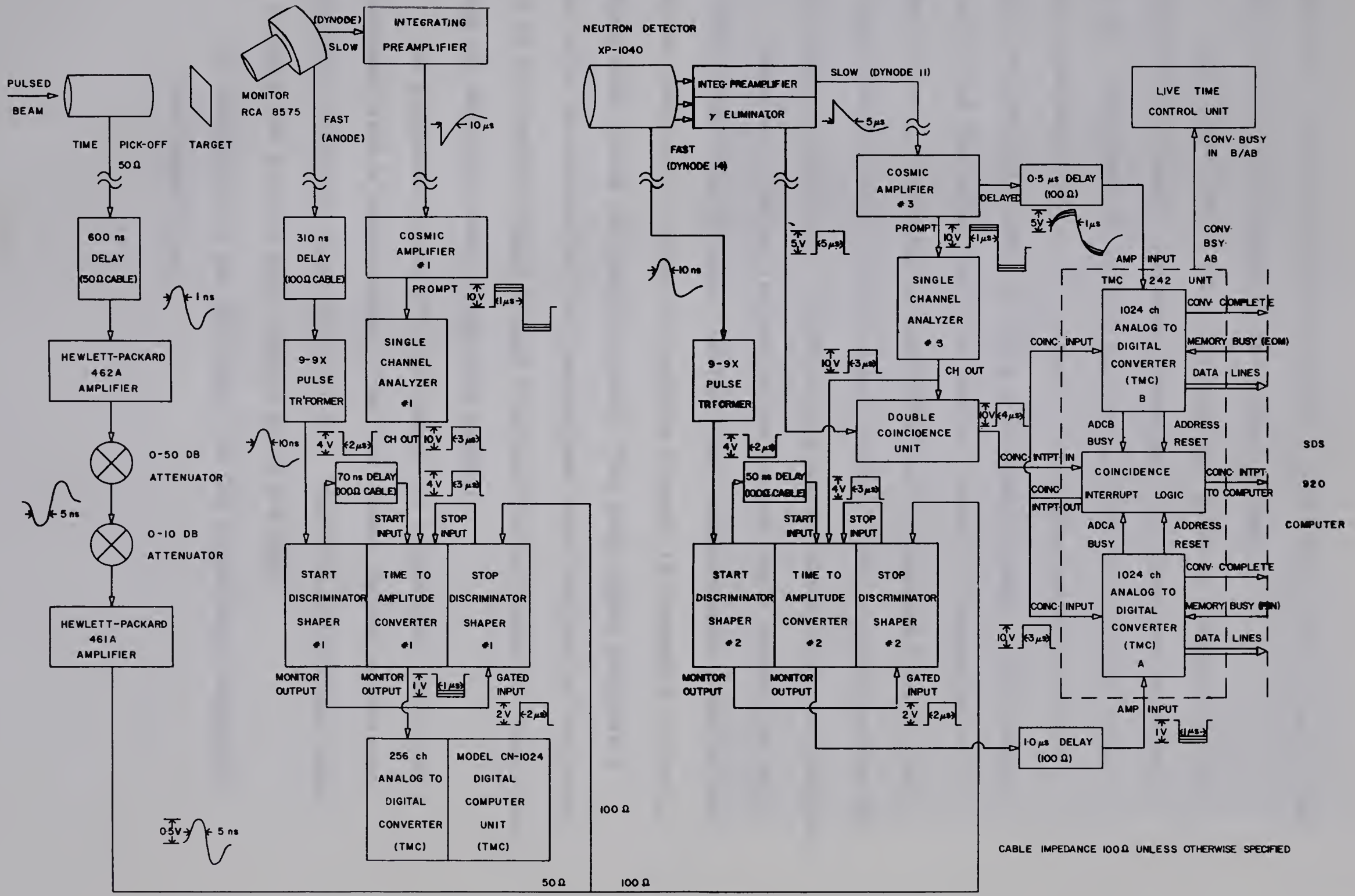

FIGURE 2-2 NEUTRON TIME OF FLIGHT SYSTEM

shielded by concrete, water and paraffin up to within 30 inches of the target chamber and thereon by two inches of lead.

The time-to-amplitude converter was based on a design by D.L. Wieber (Wi 63) using capacitance charging. The time base was about 300 ns. The output of the TAC was fed to a TMC 1024 channel pulse height analyzer (ADCA). The linear channel from dynode 11 of the XP1040 accepts only neutrons above a threshold energy. This channel is also used for pulse "walk" correction. Walk is broadening of the peaks in the spectrum due to the difference in observed timing caused by the different recoil proton pulse heights. This channel carries the pulse height information. Figure 2-2a shows an uncorrected 3-D spectrum.

Cross over timing is used in the monitor start channel as this is less susceptible to walk. Leading edge timing however gives better inherent resolution. Since the neutron channel is corrected for walk, leading edge timing is therefore used. The stop signal provides a pulse with the centroid of the passing beam burst defined by the cross-over as the induced charge swings from positive to negative. Cross-over timing is therefore used in the stop channel.

An acceptance pulse from the gamma ray eliminator (Re 66) in coincidence with a prompt signal from the linear channel enters the coincidence interrupt logic unit (Ge 66). Here the coincidence pulse has to pass the two ADS Busy inhibit gates and then

1) energize the two ADC units via the coincidence interrupt out signal, and

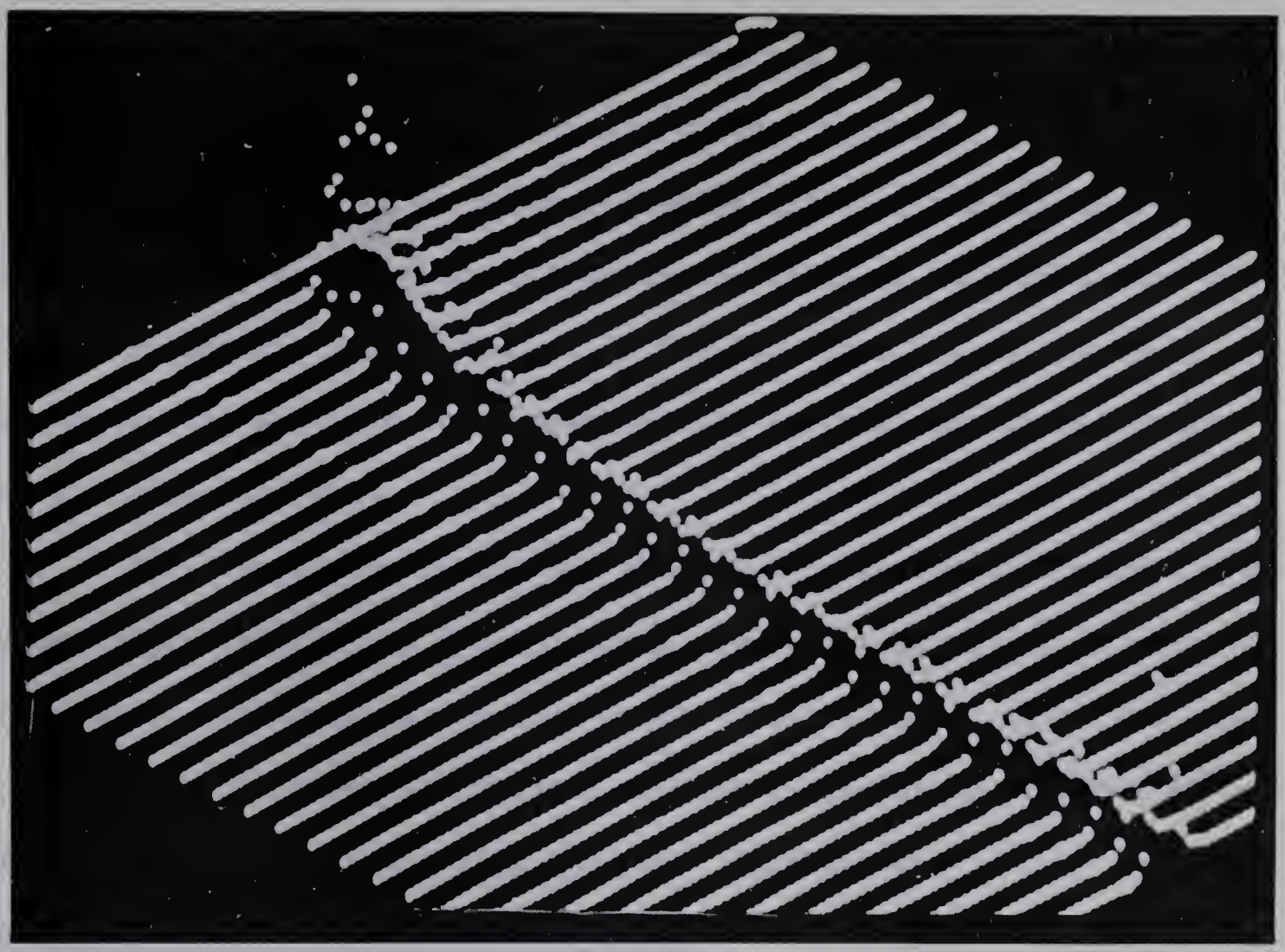

FIGURE 2–2a. AN UNCORRECTED THREE DIMENSIONAL PULSE HEIGHT DISTRIBUTION

2) in triple coincidence with the two ADC Address Reset signals energize ADC transmission to the computer.

Walk correction is accomplished by dividing the linear signal into 32 amplitude bins and finding the centroid of each bin. The distance in channels from a channel in the reference bin is the shift. The resulting shift table is read back in and the correction applied when in the NTOF mode.

The overall resolution was about 0.9 ns as compared with a previous figure of 1.25 ns (Da 66) using phototube saturation to correct for walk. The major improvement in the present method is at the base of the peaks. Using $\Delta E/E = 2\Delta t/t$ we have a resolution of about 45 keV for 5 MeV neutrons traversing a 6 meter flight path.

c. Efficiency of the Neutron Detector

The relative efficiency of the neutron detector was determined by a separate experiment using the $T(p,n)He^3$ reaction. The energy calibration of the accelerator was previously done by W.G. Davies (Da 66) using the $Li^7(p,n)Be^7$ reaction. The neutrons were detected by the main neutron detector and by a McKibben long counter with paraffin moderator (Al 60). The BF3 electronics are illustrated in Figure 2-3. The integrated count rate was corrected for counting efficiency and used as the normalization for the relative efficiency curve. The absolute efficiency was obtained from an associated particle time-of-flight experiment (Bu 66) using the $D(d,n)He^3$ reaction in conjunction with a gas target.

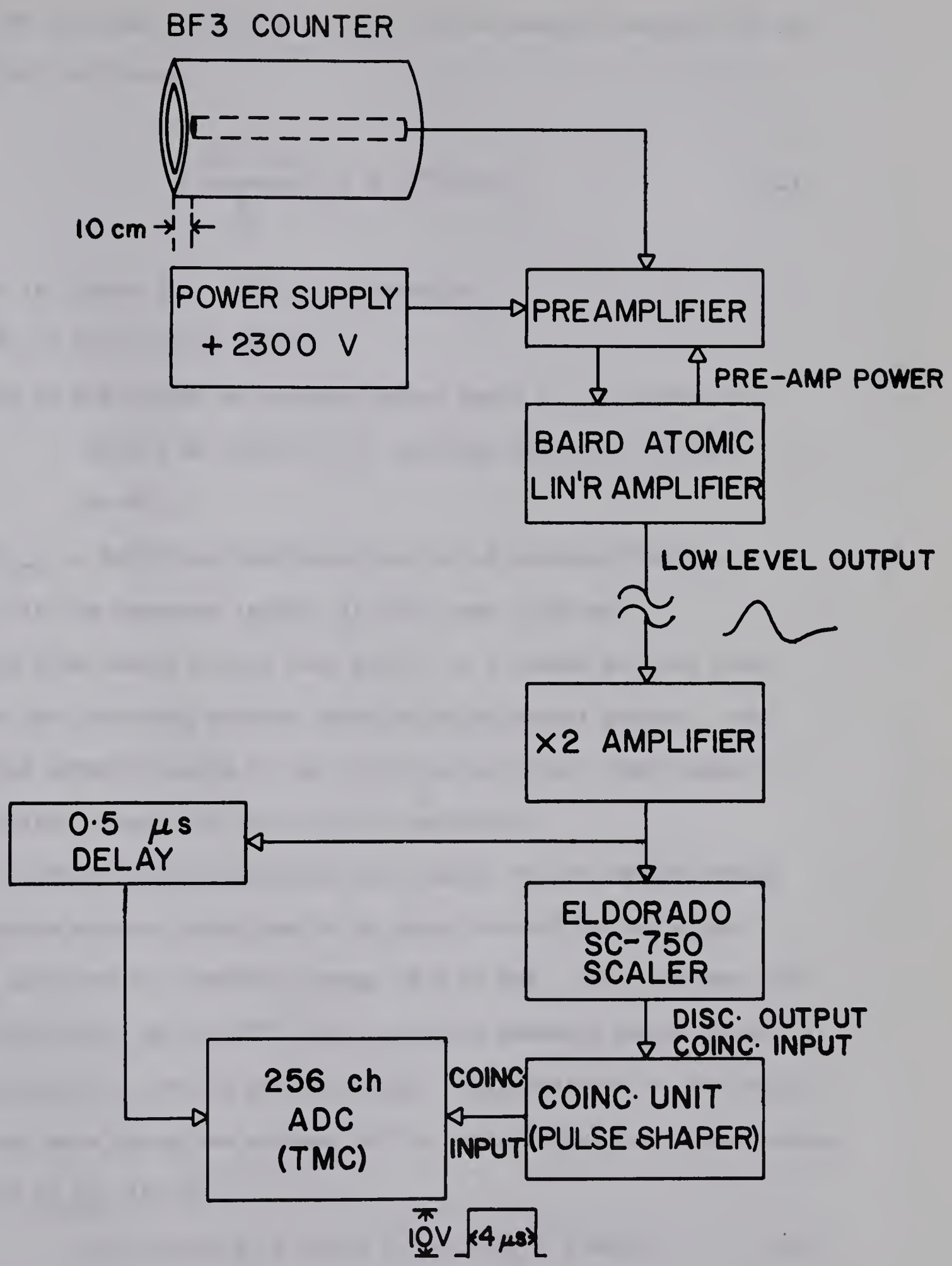

FIGURE 2-3

BF3 ELECTRONICS FOR RELATIVE EFFICIENCY MEASUREMENT

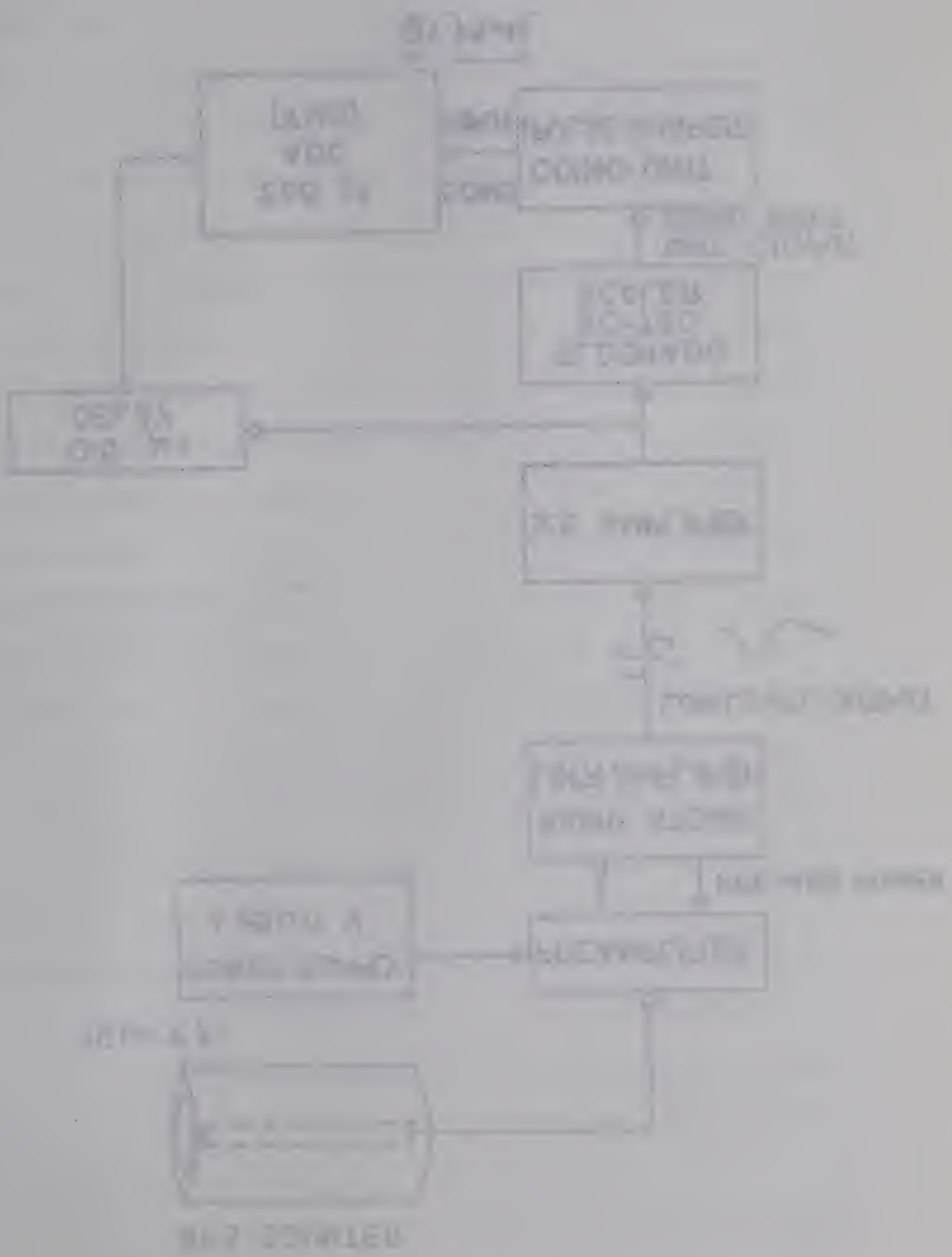

The agreement of the efficiency versus neutron energy with the theoretical efficiency

$$\left(\frac{E_n - E_o}{E_n} \right) \left(1 - e^{-n_H \sigma_{n-p} x} \right) \qquad (2\text{-}1)$$

is shown in Figure 2-4. In this expression

E_n is the neutron energy.

n_H is the number of hydrogen atoms per c.c. calculated for Ne 213 as 4.888×10^{22} hydrogen atoms/c.c. (Nu 65, Re 66).

σ_{n-p} is the total neutron-proton cross section (Ba 57).

x is the detector length, in this case 1.905 cm.

Agreement with theory is not very good. As a result a cubic interpolation was performed between smoothed experimental points. This was fitted asymptotically to the n-p cross section. There seems to be no obvious reason for this lack of agreement.

A further small correction was applied to the forward angle ground state neutron group due to an upper cut-off by the single channel analyzer at a neutron energy of 5.35 MeV. This was done with a two-dimensional $Be^9(d,n)B^{10}$ spectrum which presents pulse height vs. neutron energy vs. recoil proton energy. Extrapolation to the cut-off energy was made using the expression for pulse height vs. proton energy from Gove et al. (Go 61)

$$L_p = 0.215\ E_p + 0.028\ E_p^2 \quad (0 < E_p < 8\ \text{MeV}) \qquad (2\text{-}2)$$

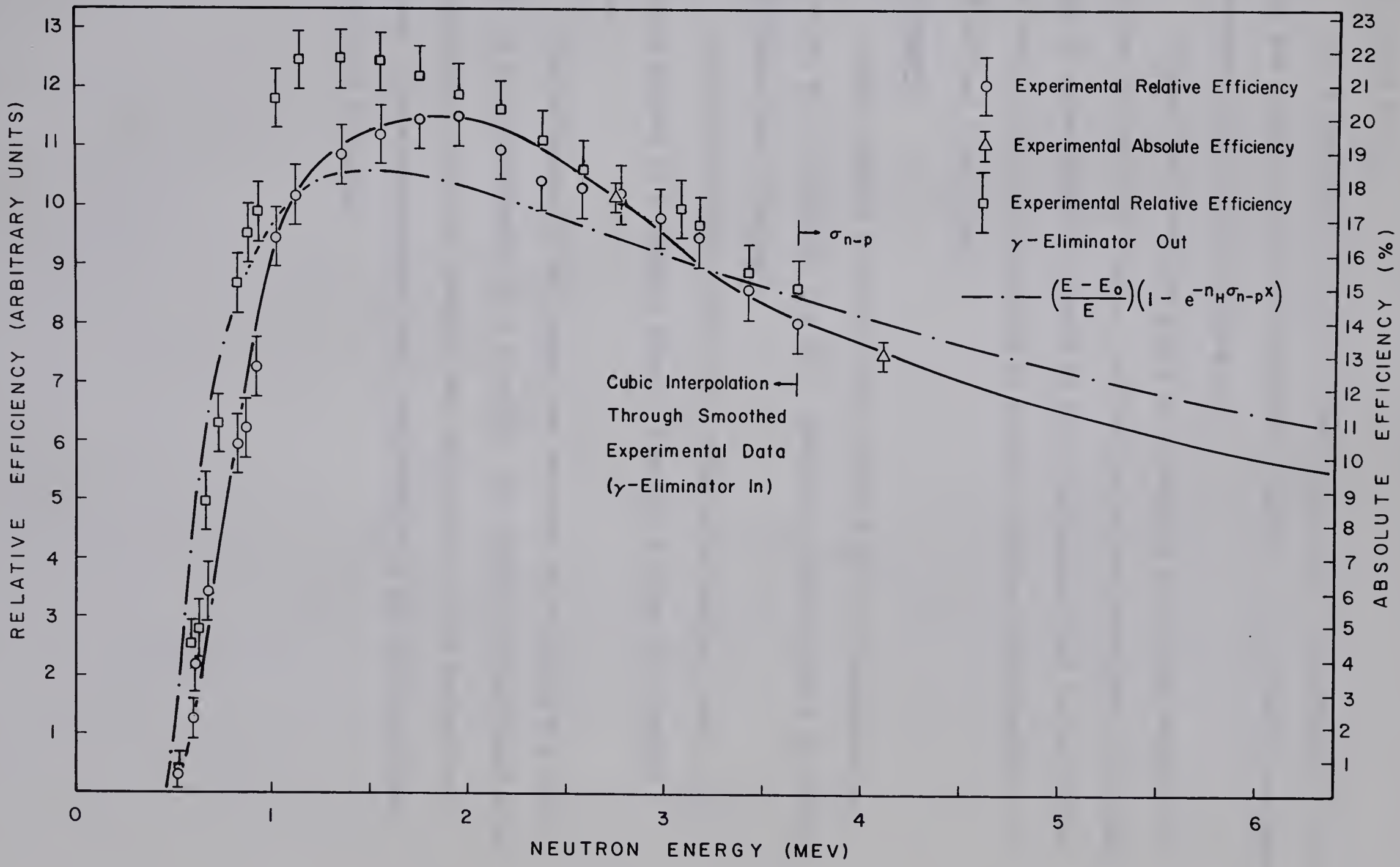

FIG. 2-4 EFFICIENCY OF THE NEUTRON DETECTOR

for liquid NE 213.

As a consistency check for future efficiency measurements a thick yield was taken from the $Mn^{55}(d,n)Fe^{56}$ reaction. A yield with the gamma eliminator in is shown in Figure 2-5.

Figure 2-6 shows the yield as a function of neutron energy for both the low and high ranges. At the time of the experiment the dynamic range of pulse heights accepted by the side channels had to be divided into two regions, corresponding to neutron energies approximately 0.5 to 5 MeV and 1 to 10 MeV.

d. Targets

Carbon targets were initially prepared by arc evaporation as described by G. Dearnaley (De 61). However it was difficult to obtain a thickness over 20 $\mu g/cm^2$.

Thin carbon targets were then prepared by smoking clean 0.005" tantalum blanks in a benzene flame. Figure 2-7 shows the benzene burner.

The thickness of the target was measured by weighing and determined to be approximately 50 ± 5 $\mu g/cm$. The target was reweighed after the experiment and then one-half and one-quarter of the target were weighed. These measurements were consistent with the previous determination of 50 $\mu g/cm^2$.

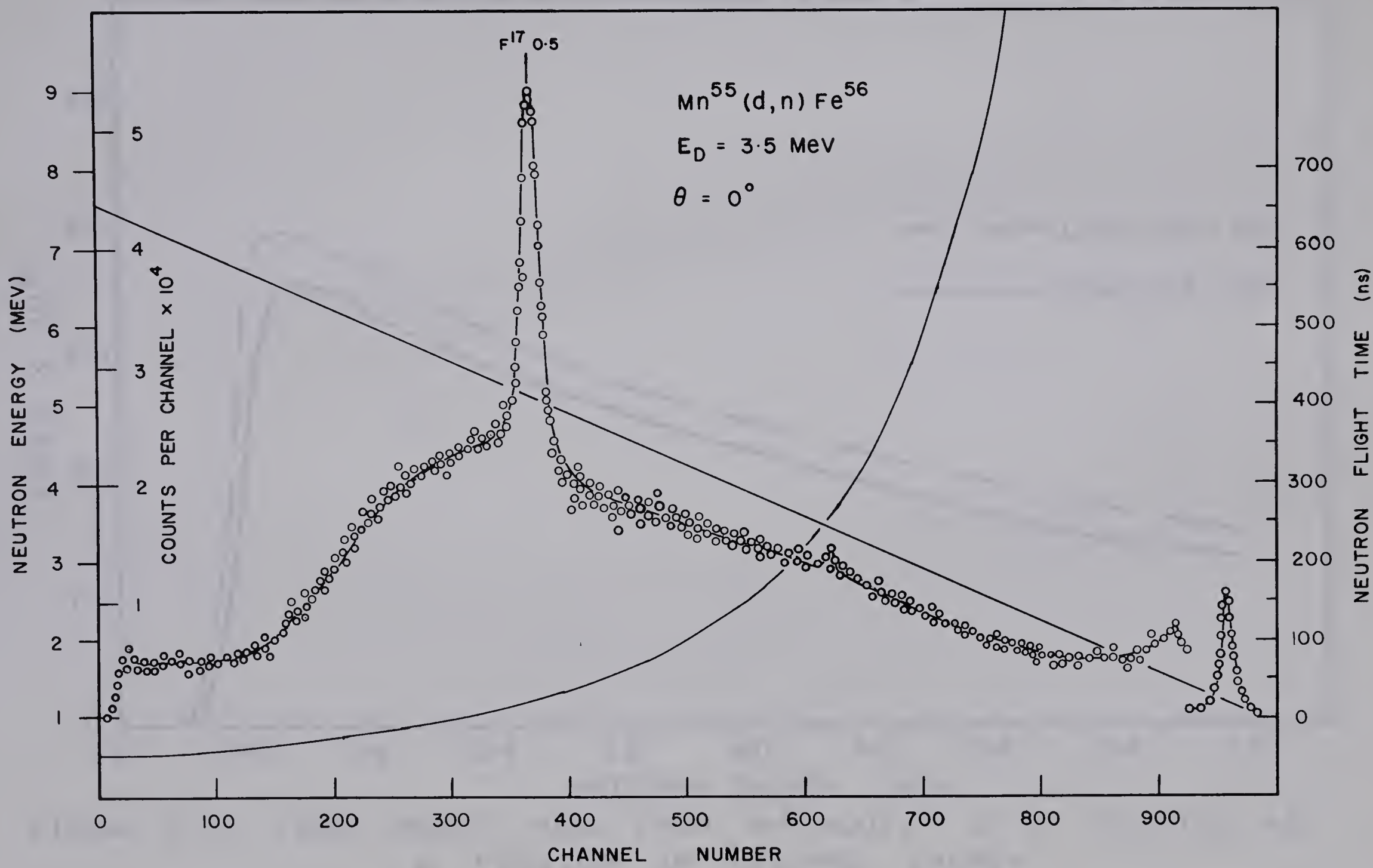

FIG· 2-5 THICK TARGET YIELD

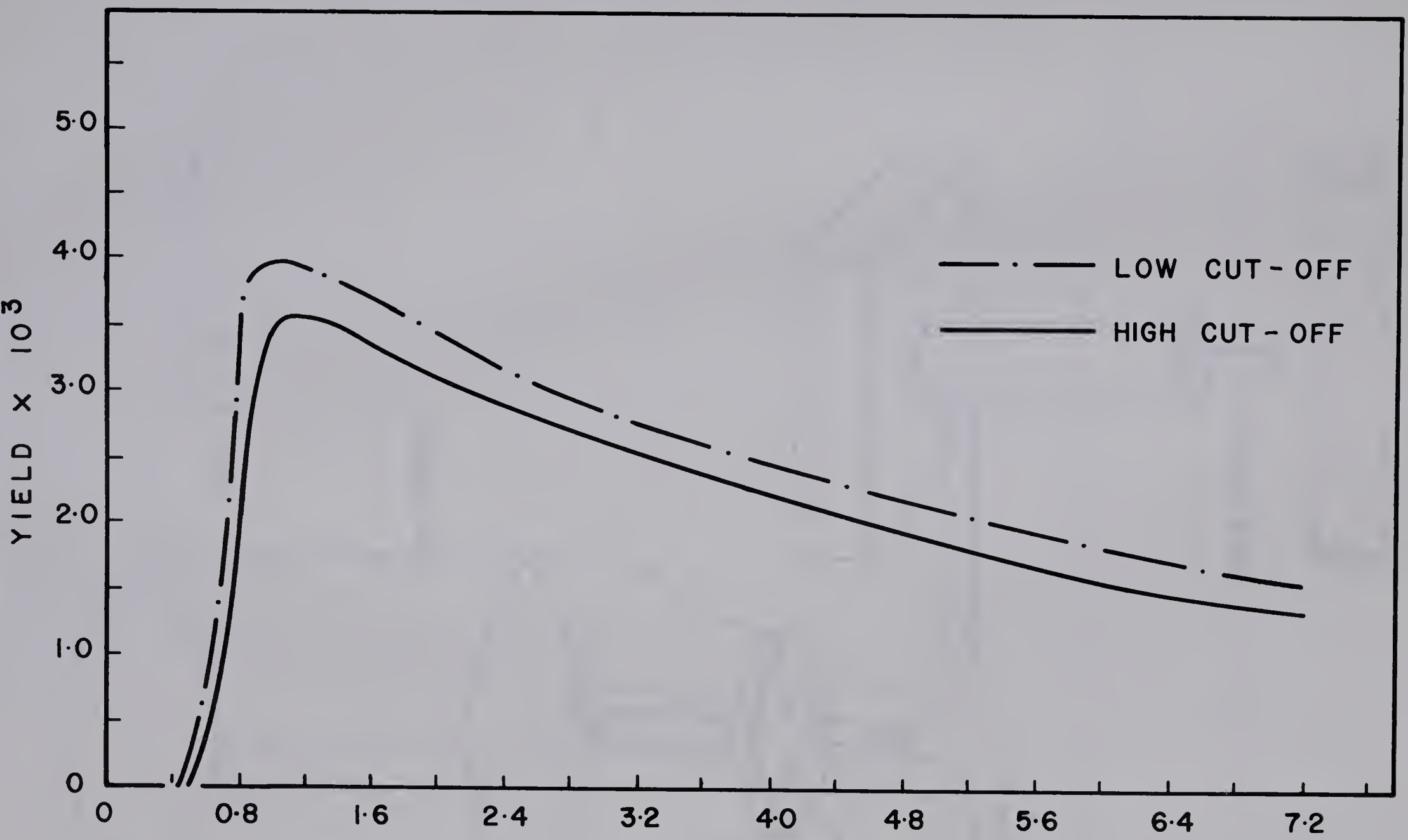

FIGURE 2-6· THICK TARGET YIELD FROM $Mn^{55}(d,n)Fe^{56}$ AT 0° PLOTTED AS A FUNCTION OF NEUTRON ENERGY

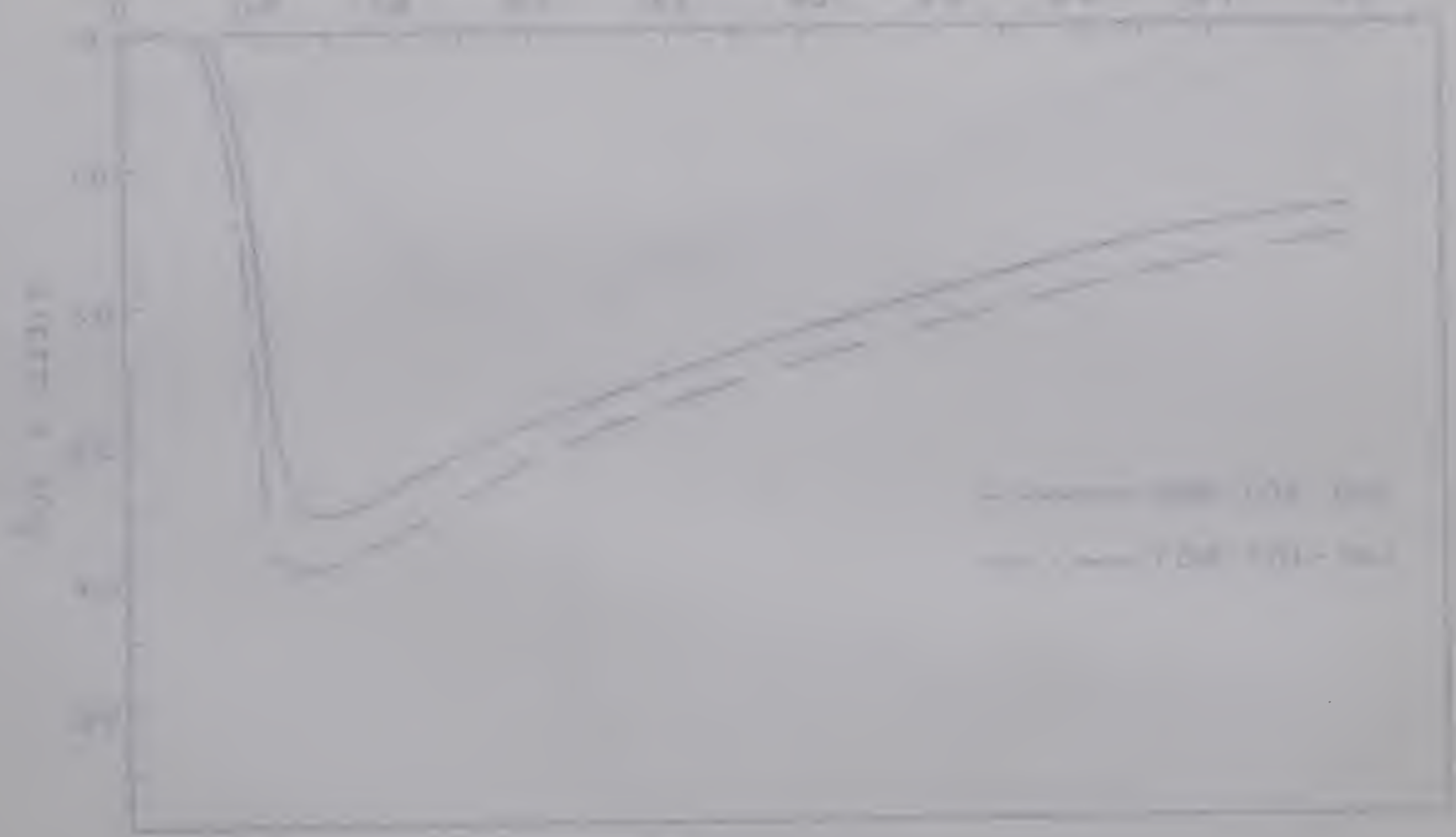

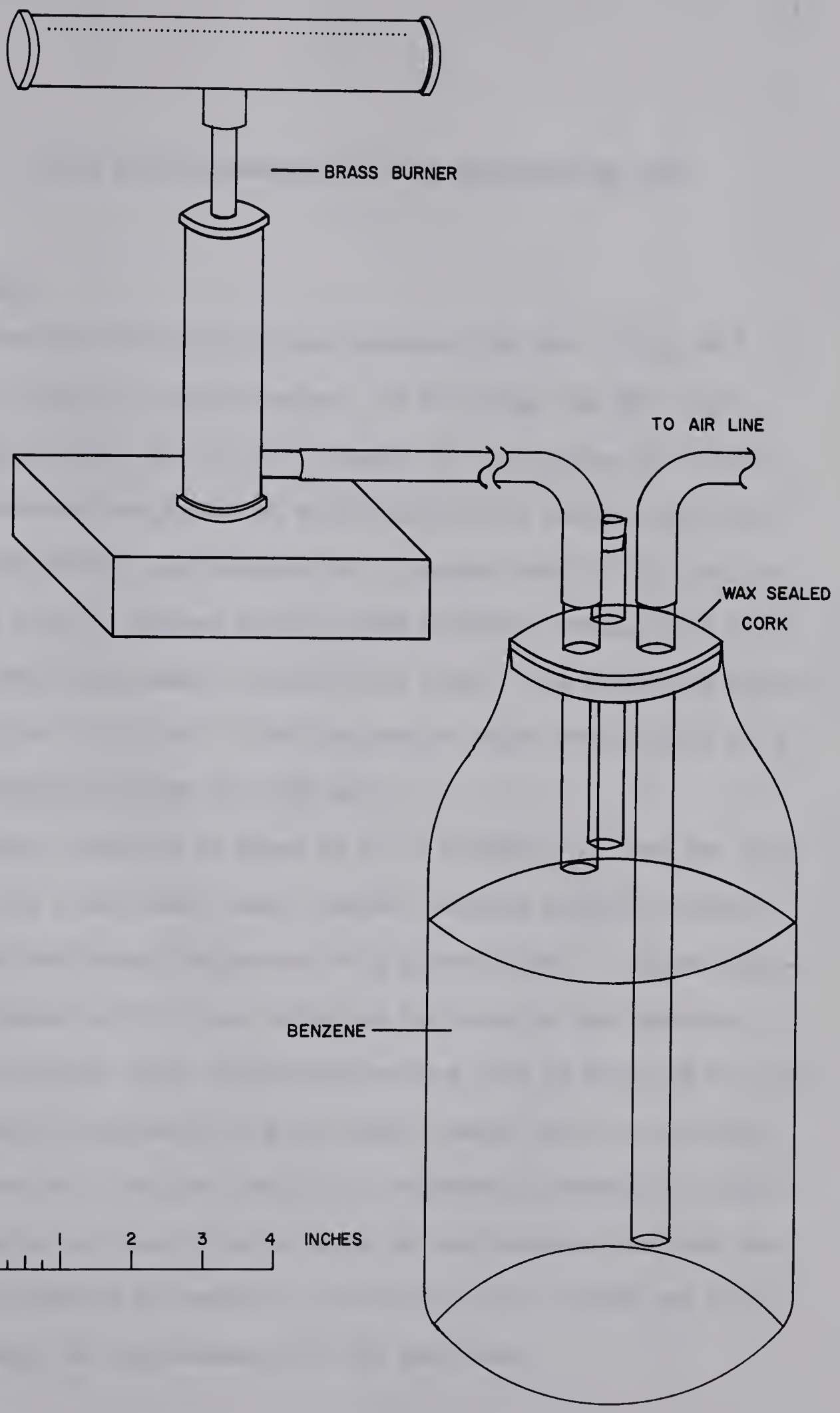

FIGURE 2-7 BENZENE BURNER

III. DATA ANALYSIS-AQUISITION AND REDUCTION OF DATA

a. Procedure

Angular distributions of the neutrons from the $C^{12}(d,n)N^{13}$ reaction were taken at twenty angles: in 5° steps from 0° to 65° and in 10° steps from 75° to 145°, except for two angles at 35° and 55°. The detector was placed at a distance of six meters from the target and the monitor was located at 1.5 meters and -30°. The live times of the monitor channel and the main detector channel were recorded and these were used to correct the yield. The analyzing magnet NMR averaged out to 29.296 ± 0.001 megacycles which corresponds to a deuteron bombarding energy of 5.994 MeV.

A typical spectrum is shown at 0° in Figure 3-1. The raw data was fitted with a nonlinear least squares Gaussian fitting program (Da 66) which subtracted background of a given shape. A linear background was chosen as this least affected the area of the Gaussian. The Gaussian in most cases underestimated the area by about 5% as there was no skewness compensation and the actual peaks were more pointed, although a variable standard deviation compensated somewhat for this. The fitted areas were nevertheless used as the computer was more consistent. Furthermore the monitor spectrum was also fitted and this tended to cancel an underestimate of the peak area.

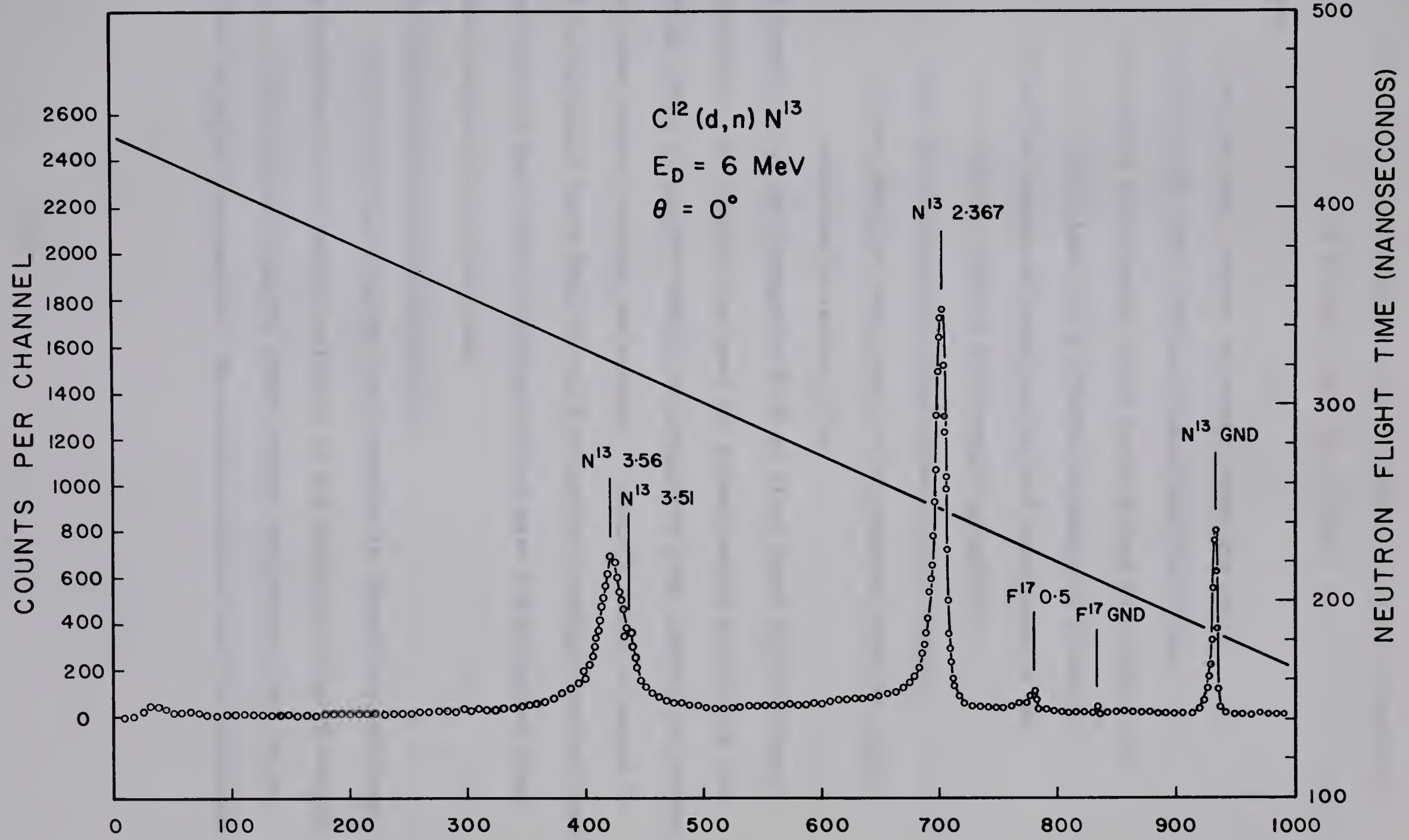

FIGURE 3-1 $C^{12}(d,n)N^{13}$ SPECTRUM AT 0°

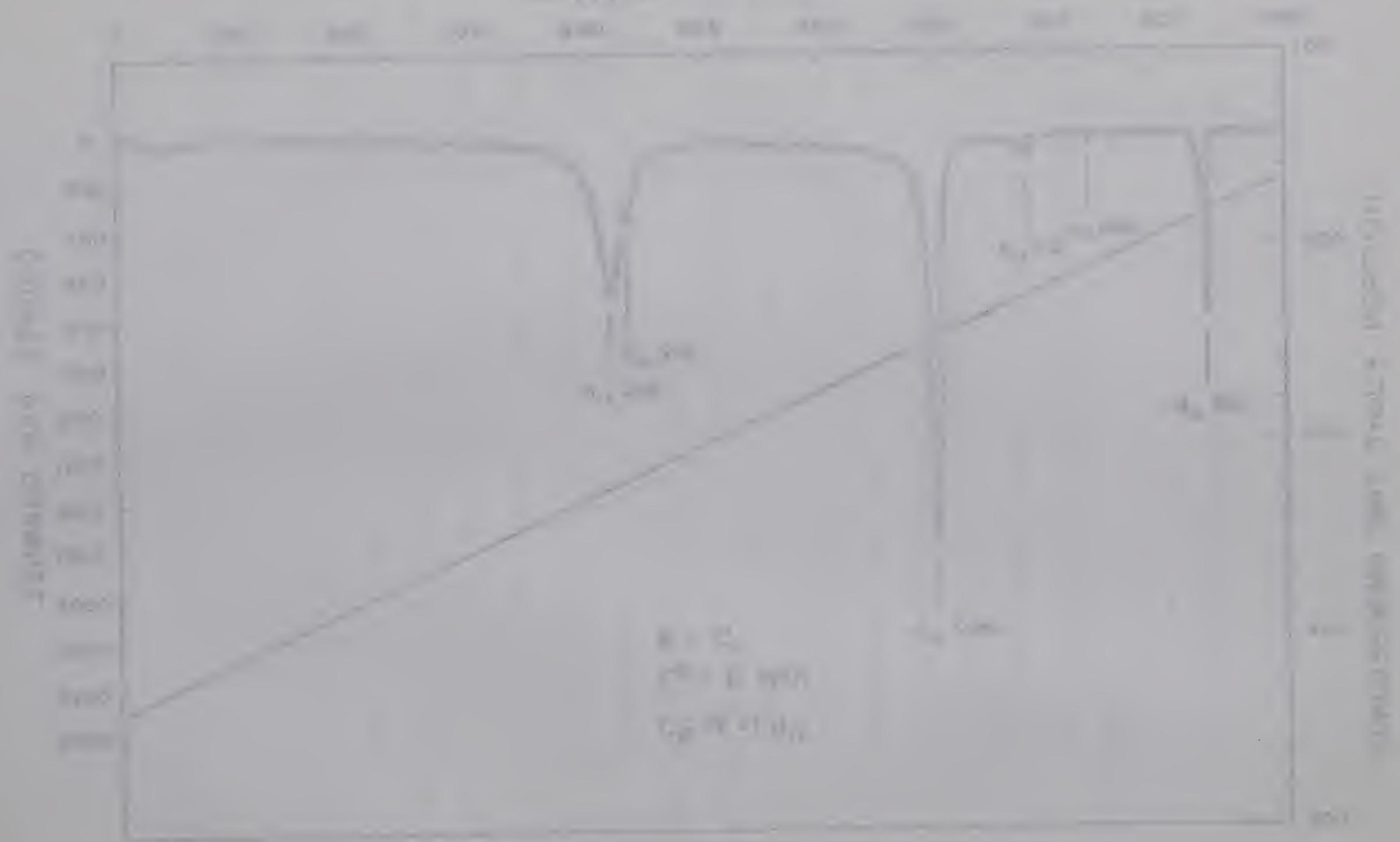

Absolute cross sections were calculated from the expression

$$C = \sigma(\theta) \cdot d\Omega \cdot N \cdot \int Idt \cdot \varepsilon \qquad (3\text{-}1)$$

where

C is the total number of counts under the peak.

$\sigma(\theta)$ is the cross section in millibars/steradian.

$d\Omega$ is the solid angle, which in this case was 1.666×10^{-4} steradians for a detector distance of 6 meters.

N is the number of target nuclei/cm^2 calculated to be $(2.59 \pm 0.26) \times 10^{18}$ target nuclei/cm^2.

$\int Idt$ is the integrated beam current on the target.

ε is the absolute efficiency of the neutron detector calculated as in section II b.

The beam current was integrated with an Elcor Model A309A current integrator. The monitor was used for normalization by finding the average ratio of monitor counts to integrated beam current for several runs where double pulsing was minimal. Double pulsing is caused by the elliptically swept beam at the top terminal passing over the aperture twice in each cycle. This ratio then gave the corrected integrated current for all the runs.

b. The 3.51-3.56 MeV Doublet in N^{13}

The two states involved were essentially unresolved, although the presence of the weakly excited 3.51 MeV state was clearly noticeable. The nonlinear Gaussian least squares program was used in an effort to split this doublet. No previous neutron work has succeeded

in splitting the two states, and this is further complicated by the fact that while these two states are only 50 keV apart, they are respectively 63 and 61 keV wide (Aj 59).

There were two methods of approaching the problem. One was to obtain the peak means from a time calibration line extracted from a Beryllium reference spectrum. The Beryllium peaks, however, were situated at the high energy end of the kicksorter and the known nonlinearity of the ADC would render extrapolation meaningless.

Alternatively one could assume that the 3.51 MeV state is weakly excited with respect to the 3.56 MeV state and, assuming two Gaussians, search for the best peak means. The weak excitation of the 3.51 MeV level is evidenced in the mirror levels in C^{13} at 3.68 and 3.85 MeV where McGruer *et al.* (Mc 55) found that $\sigma_{3.855}(\theta)/\sigma_{3.685}(\theta)$ is 9.5. From elastic proton scattering on C^{12} Jackson and Galonsky (Ja 51) found a ratio of 6.3 for the reduced widths of the 3.56 to 3.51 MeV levels.

With this in mind the best fit mean to the 3.56 MeV state, keeping the standard deviations fixed, was taken to be the true mean of that level. The position of the 3.51 MeV level was fixed by finding the number of channels corresponding to the known kinematic time difference (Gr 65) and interpolating for the curve in Figure 3-2 corresponding to an ADCA baseline setting of 0.1. This technique yielded means for the 3.51 MeV state consistent with a visual estimate. The integral linearity of the analog to digital converter is shown in Figure 3-3.

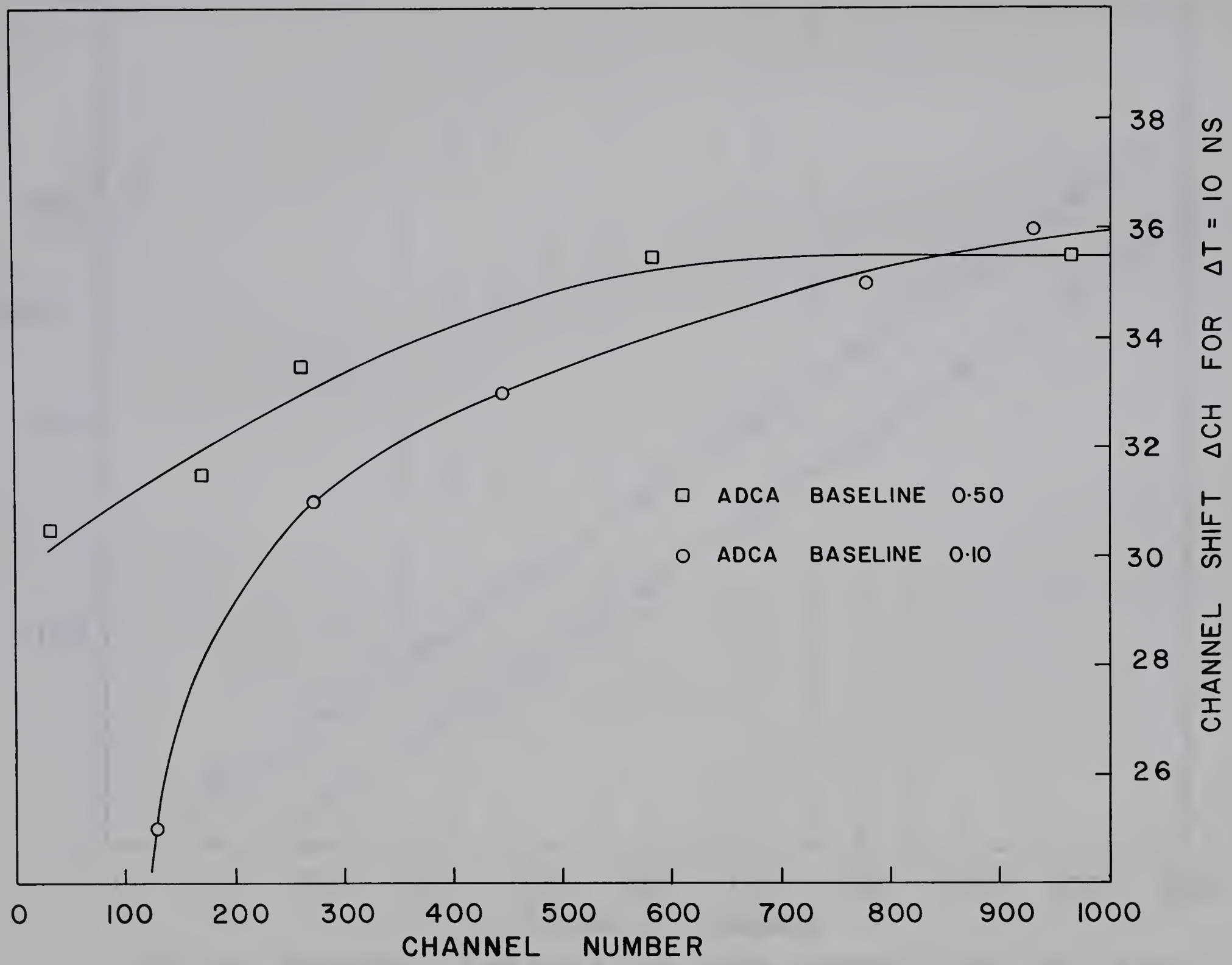

FIG·3-2 DIFFERENTIAL LINEARITY OF TIME CHANNEL ADC (Courtesy W·J· McDonald)

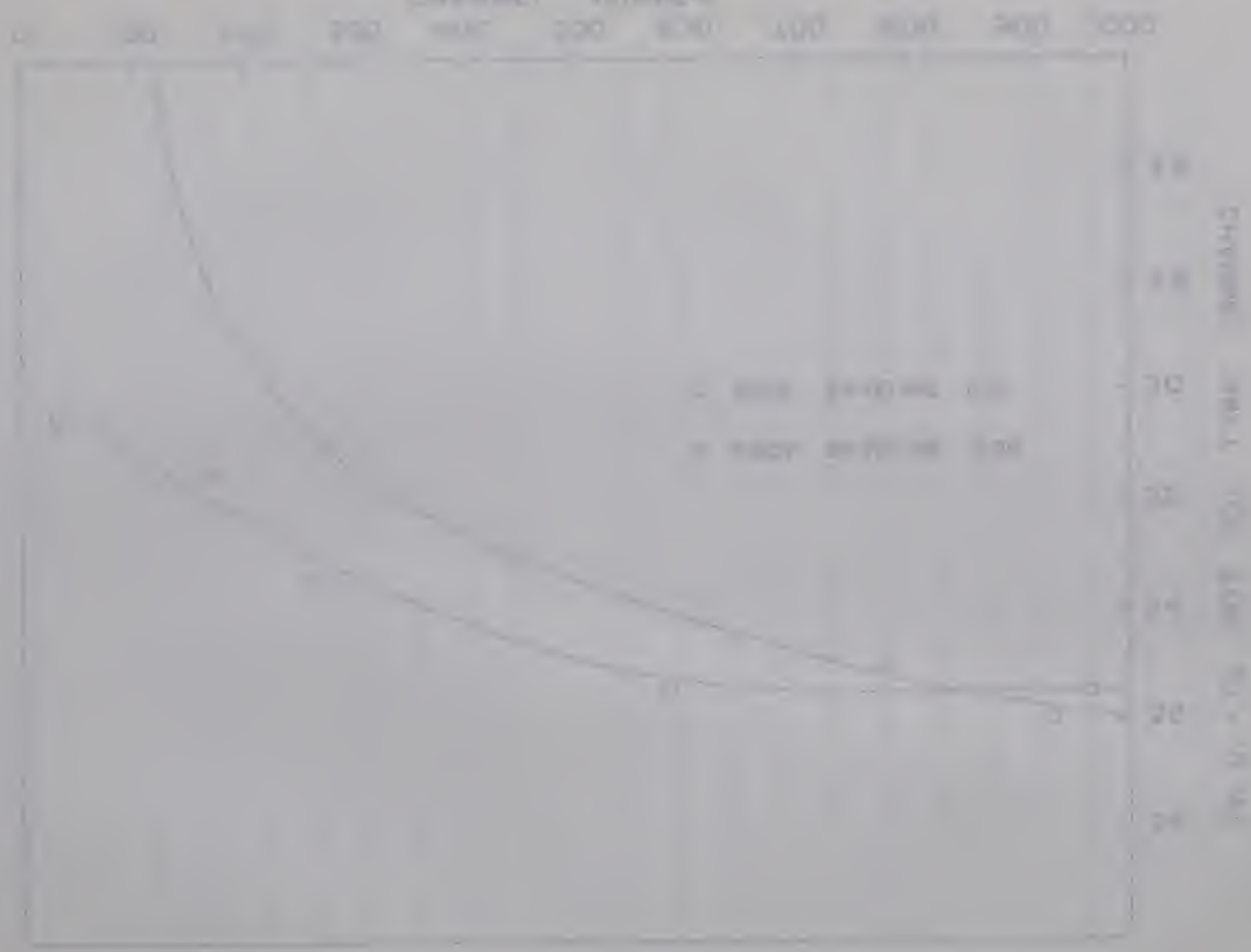

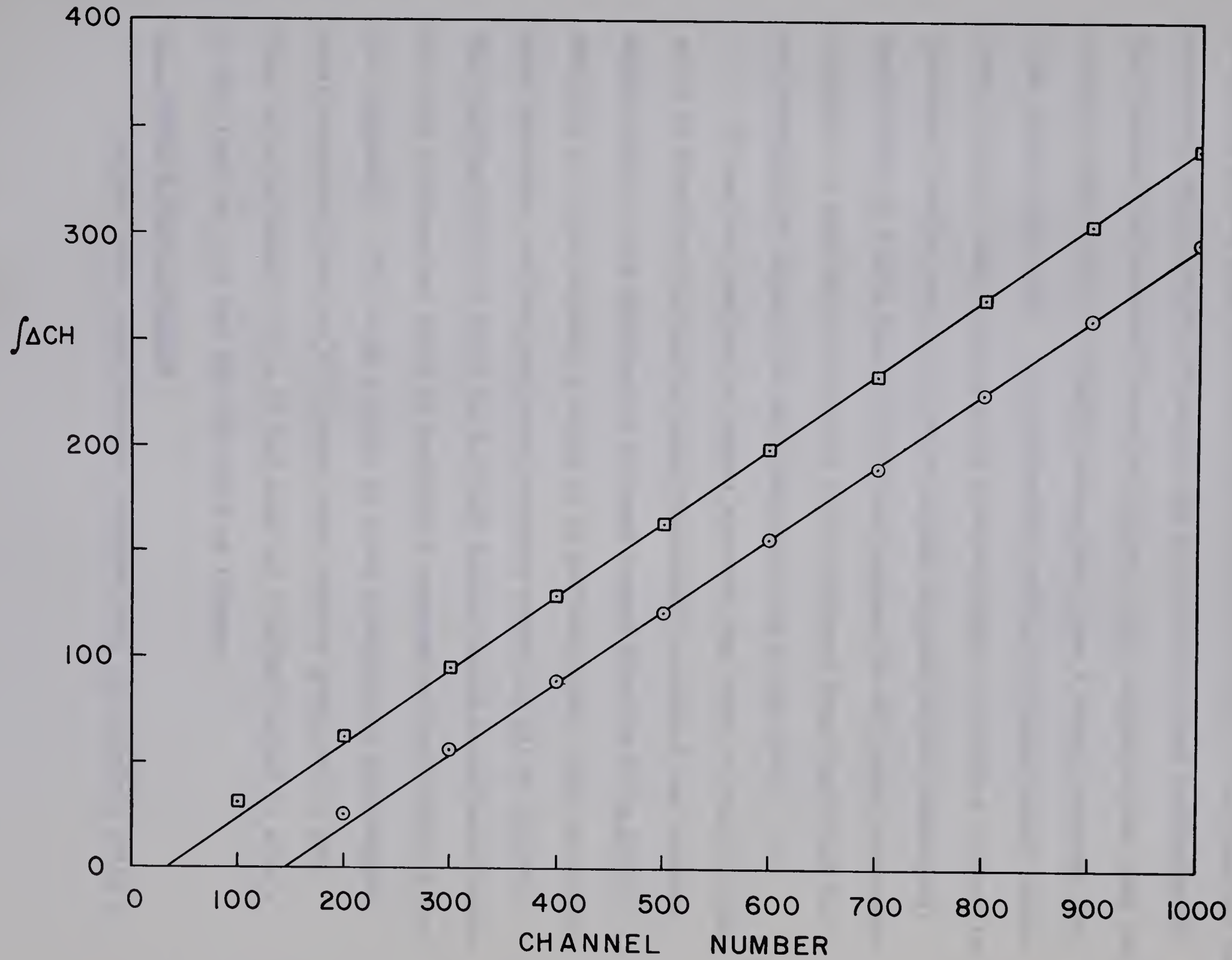

FIG·3-3 INTEGRAL LINEARITY OF TIME CHANNEL ADC (See Fig·3-2)

Since these two states have almost the same width, this parameter was fixed to the same constant in the fitting procedure. The shape of the extracted angular distribution for the 3.51 MeV state was unaffected by the value of the standard deviation chosen. This indicates that what was actually extracted was probably nothing more than a fairly constant portion of the total peak. The instrumental width, including target thickness, was much less than the total observed width. Therefore further improvement in time resolution is not likely to yield better separation. Application of a more realistic fitting program (Te 66) might prove more fruitful. A time calibration line to fix the peak means was tried but the extrapolated means were too uncertain to be of any use.

It was not possible to deduce directly the width of the 2.367 MeV state as there were no nearby peaks from which to extract the instrumental width. With neutrons of the same energy from the $Li^7(p,n)Be^7$ reaction for this purpose, a width of 49 keV was found. This is not in good agreement with the previously reported value (Aj 59) of 32 keV. The combined width of the 3.51-3.56 MeV doublet could be estimated since here the instrumental width is negligible compared to the widths of the two components. The value arrived at after unfolding an instrumental width extracted from the N^{13} ground state neutron group was 71 keV. This is in agreement with a 61 keV level at 3.56 MeV folded in with a 63 keV level at 3.51 MeV and one-sixth as intense.

c. Absolute Cross Sections

Absolute cross sections were obtained from the raw data using a

computer program written by Mr. T.B. Grandy which corrected the measured intensities for neutron attenuation in the gold backing and made the necessary laboratory to center of mass transformation. The overall normalization was obtained using the procedure of section III a. The efficiency subroutine was rewritten to accomodate a cubic interpolation asymptotic to the σ_{n-p} cross section. Tables III-1 to III-5 list the absolute cross sections found in this experiment.

The relative errors shown in the tables are in absolute units. These errors are from the Gaussian fitting program and from the efficiency. Not shown is the overall normalization error arising from target thickness and beam integration. This adds another 10% error giving a total error of about 20%.

Table III-3 contains the combined doublet in N^{13}. This is taken to be the cross section for the 3.56 MeV component for the reasons outlined in section III b. Tables III-4 and III-5 contain the cross sections for each component of the doublet, as separated by the Gaussian fitting program. The total errors in these values are much larger, that for the 3.51 MeV level is probably between 50% and 100%.

ABSOLUTE CROSS SECTIONS FOR $C^{12}(d,n)N^{13}$
TO THE GROUND STATE AT E_D = 5.994 MEV

Angle (Lab)	Angle (C. of M.)	Cross Section (mb/sr)	Relative Error
0.0	0.0	20.96	1.95
5.0	5.6	21.35	2.20
10.0	11.2	23.06	2.15
15.0	16.7	19.42	1.96
20.0	22.3	18.30	1.66
25.0	27.9	11.95	1.14
30.0	33.4	7.02	0.70
40.0	44.3	2.86	0.25
45.0	49.8	1.76	0.18
50.0	55.1	2.11	0.18
60.0	65.9	3.24	0.27
65.0	71.1	3.99	0.33
75.0	81.5	3.98	0.30
85.0	91.7	2.86	0.23
95.0	101.7	2.71	0.22
105.0	111.5	2.34	0.20
115.0	121.1	2.88	0.23
125.0	130.5	3.66	0.30
135.0	139.8	3.21	0.35
145.0	148.9	3.37	0.36

Table III - 1

ABSOLUTE CROSS SECTIONS FOR $C^{12}(d,n)N^{13}$
TO THE 2.367 MEV STATE AT E_D = 5.994 MEV

Angle (Lab)	Angle (C. of M.)	Cross Section (mb/sr)	Relative Error
0.0	0.0	57.37	4.50
5.0	5.8	56.27	5.09
10.0	11.6	44.10	3.52
15.0	17.4	25.71	2.33
20.0	23.2	18.01	1.41
25.0	29.0	8.26	0.72
30.0	34.7	5.64	0.49
40.0	46.1	5.34	0.38
45.0	51.7	5.04	0.40
50.0	57.2	5.33	0.36
60.0	68.2	4.54	0.32
65.0	73.6	3.58	0.25
75.0	84.1	3.46	0.23
85.0	94.4	3.20	0.22
95.0	104.4	3.66	0.26
105.0	114.1	3.83	0.28
115.0	123.6	3.97	0.28
125.0	132.7	4.00	0.28
135.0	141.7	3.13	0.23
145.0	150.4	2.81	0.21

Table III - 2

ABSOLUTE CROSS SECTIONS FOR $C^{12}(d,n)N^{13}$ TO THE 3.56 NEV STATE (UNSEPARATED) AT E_D = 5.994 MEV

Angle (Lab)	Angle (C. of M.)	Cross Section (mb/sr)	Relative Error
0.0	0.0	41.65	3.15
5.0	6.1	45.87	4.00
10.0	12.3	40.53	3.11
15.0	18.4	30.52	2.66
20.0	24.5	30.98	2.35
25.0	30.5	21.19	1.76
30.0	36.5	19.27	1.57
40.0	48.4	14.07	0.95
45.0	54.3	8.68	0.67
50.0	60.1	7.51	0.49
60.0	71.4	4.68	0.33
65.0	76.9	3.35	0.24
75.0	87.7	3.55	0.24
85.0	98.1	4.42	0.31
95.0	108.1	6.28	0.43
105.0	117.7	7.36	0.53
115.0	126.9	10.15	0.76
125.0	135.8	7.10	0.57
135.0	144.3	6.97	0.61
145.0	152.5	6.15	0.57

Table III - 3

ABSOLUTE CROSS SECTIONS FOR $C^{12}(d,n)N^{13}$ TO THE 3.56 MEV STATE (SEPARATED) AT E_D = 5.994 MEV

Angle (Lab)	Angle (C. of M.)	Cross Section (mb/sr)	Relative Error
0.0	0.0	28.58	2.23
5.0	6.1	35.92	3.18
10.0	12.3	30.84	2.42
15.0	18.4	24.32	2.17
20.0	24.5	25.03	1.93
25.0	30.5	15.39	1.32
30.0	36.5	14.40	1.20
40.0	48.4	11.11	0.77
45.0	54.3	6.48	0.52
50.0	60.1	5.25	0.35
60.0	71.4	3.53	0.25
65.0	76.9	2.49	0.18
75.0	87.7	2.98	0.95
85.0	98.1	3.24	0.23
95.0	108.0	4.18	0.29
105.0	117.7	6.06	0.44
115.0	126.9	6.29	0.47
125.0	135.8	5.39	0.42
135.0	144.3	4.97	0.38
145.0	152.5	4.86	0.39

Table III - 4

ABSOLUTE CROSS SECTIONS FOR $C^{12}(d,n)N^{13}$ TO THE 3.51 MEV STATE (SEPARATED) AT E_D = 3.51 MEV

Angle (Lab)	Angle (C. of M.)	Cross Section (mb/sr)	Relative Error
0.0	0.0	9.45	0.89
5.0	6.1	7.09	0.83
10.0	12.2	6.71	0.73
15.0	18.3	6.01	0.72
20.0	24.4	4.66	0.51
25.0	30.4	4.16	0.46
30.0	36.4	3.62	0.62
40.0	48.3	2.15	0.23
45.0	54.1	1.97	0.23
50.0	59.9	1.59	0.15
60.0	71.2	0.93	0.10
65.0	76.7	0.60	0.09
75.0	87.5	0.51	0.09
85.0	97.9	0.92	0.12
95.0	107.9	1.51	0.15
105.0	117.5	0.92	0.20
115.0	126.7	1.76	0.22
125.0	135.6	0.98	0.21
135.0	144.1	0.98	0.19
145.0	152.4	0.95	0.16

Table III - 5

IV. DATA ANALYSIS-INTERPRETATION OF DATA

a. Plane Wave Analysis

The angular distribution extracted from the observed levels of N^{13} were analyzed with the plane wave Born approximation using the programmed Lubitz (Lu 57) calculation. In the case of capture into unbound levels of the final nucleus, however, it is very difficult to determine the ℓ-value of the captured particle (Ma 60).

This difficulty is born out in the present experiment (Figure 4-1). For the unseparated neutron group at 3.51-3.56 MeV excitation in N^{13} $\ell_p = 1$ and $\ell_p = 2$ fitted equally well. If a radius parameter between $r_p = 3.5$ f and $r_p = 8.0$ f is acceptable, consistent with the literature (Ma 60, Da 52), then $\ell_p = 1 (r_p = 3.0$ f) is excluded in favor of $\ell_p = 2$ ($r_p = 5.5$ f).

Plane wave fits to the separated components of the 3.51-3.56 MeV doublet (Figure 4-2) are more ambiguous in the choice of ℓ-value. This possibly reflects the uncertainty in the separation procedure (Chapter III) rather than ambiguity in the theory. No conclusion can be drawn on the best ℓ-value. The same is true of the fit to the 3.51 MeV state.

A further difficulty arises in dealing with $\ell = 0$ capture into levels of the final nucleus close to the nucleon separation energy

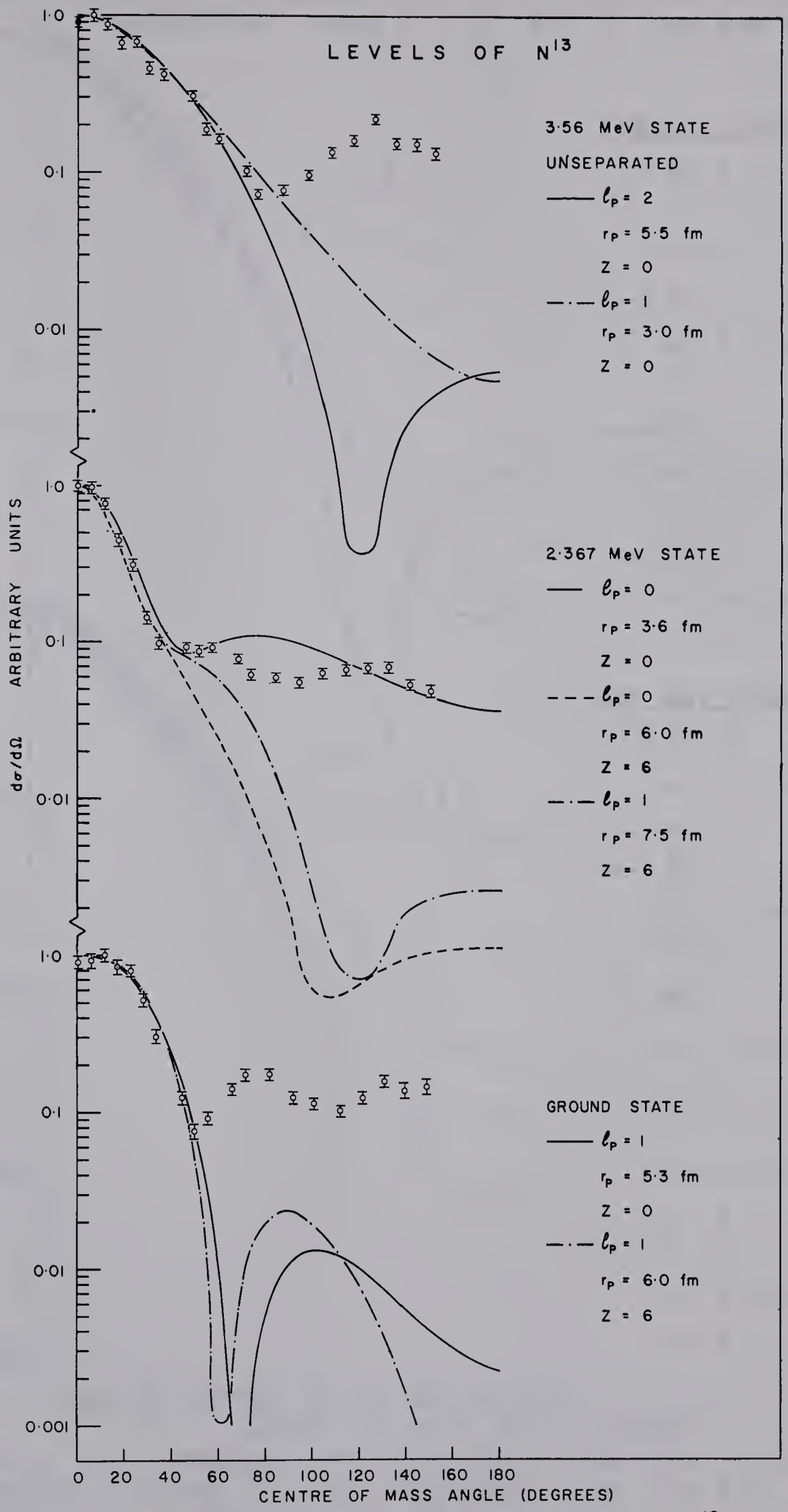

FIGURE 4-1· ANGULAR DISTRIBUTIONS FROM THE $C^{12}(d,n)N^{13}$ REACTION LEADING TO THE GROUND ($J^{\pi} = 1/2^{-}$), 2·367 ($J^{\pi} = 1/2^{+}$), AND UNSEPARATED 3·56 ($J^{\pi} = 5/2^{+}$)· MEV STATES OF N^{13} AT E_D = 5·994 MEV

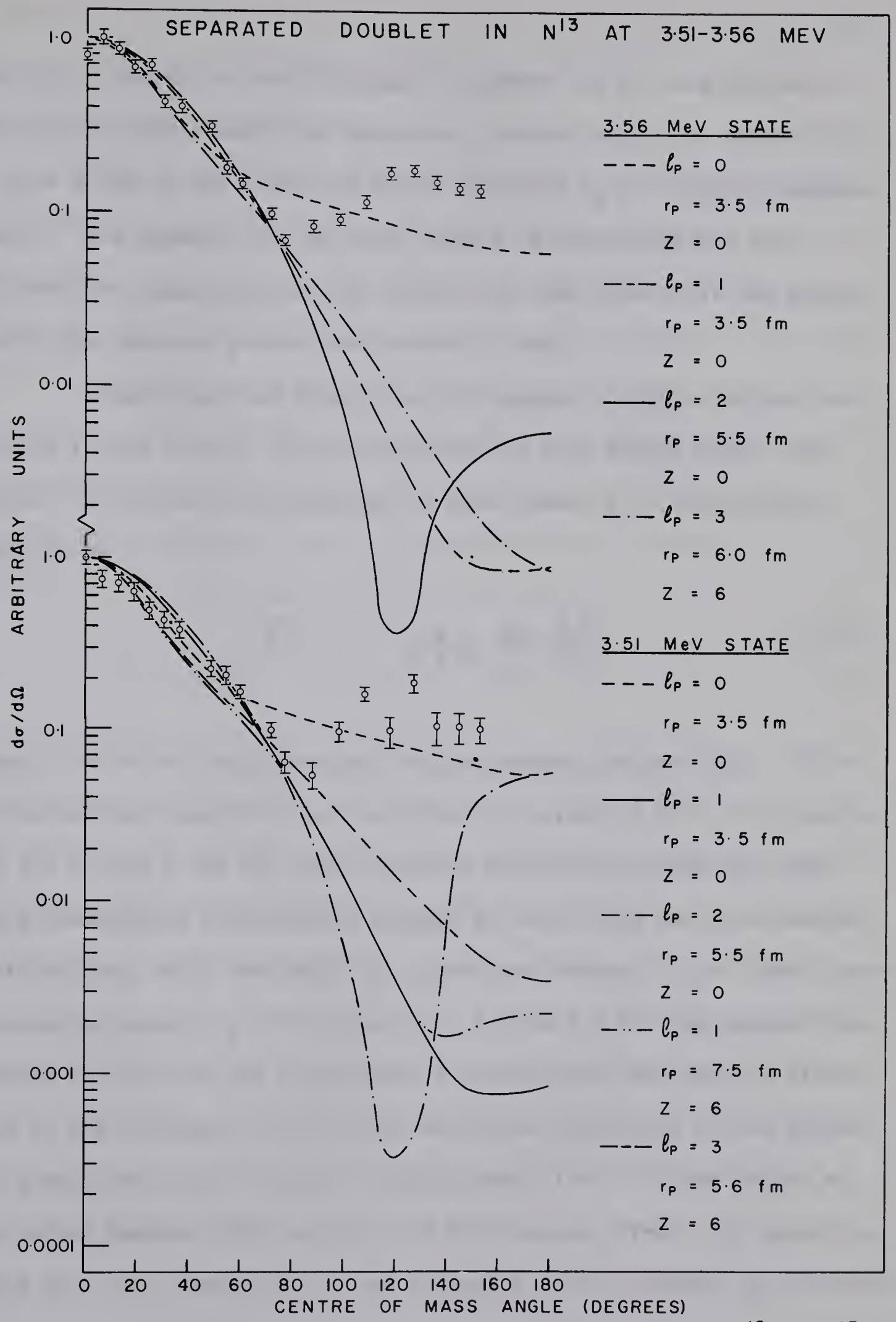

FIGURE 4-2 ANGULAR DISTRIBUTIONS FROM THE $C^{12}(d,n)N^{13}$ REACTION LEADING TO THE SEPARATED 3·51 ($J^{\pi} = 3/2^{-}$) AND 3·56 ($J^{\pi} = 5/2^{+}$) MEV STATES OF N^{13} AT E_D = 5·994 MEV PLANE WAVE FITS ARE SHOWN

(Ma 60). Contrary to the findings of Calvert (Ca 57) and Middleton (Mi 53) who used 9 and 8 MeV deuterons, respectively, the present fit at E_D = 6 MeV to the 2.367 MeV level indicates $\ell_p = 0$ capture unambiguously. The apparent fit at large angles is misleading and only reflects the singularity of the theory for that level. At the singularity the captured proton wave number is zero.

MacFarlane and French (Ma 60) suggest a simple Coulomb correction in the case of (d,n) transitions to such weakly bound final states. This involves replacing the wave number t of the captured particle by

$$\overline{t}^2 = t^2 + \frac{A}{A+1}\,\frac{2M}{h^2}\,\frac{Ze^2}{r_o} \qquad \text{(IV-1)}$$

where A and M are the target and nucleon masses, respectively. This correction was applied to all the observed levels of N^{13}. The resulting fit to the 2.367 MeV level improved stability in that the large angle theoretical distribution dropped to well below the experimental distribution, as is customary for plane wave theory. $\ell_p = 0$ had a more reasonable radius, r_p = 6 f, than $\ell_p = 1$ with 7.5 f. The Coulomb correction did not fit the unseparated 3.56 MeV level and made no difference to the ambiguous fits for the separated components of the doublet. The ground state distribution, unambiguously $\ell = 1$, fitted better at the second maximum with inclusion of the Coulomb effect. It should be noted that with increasing ℓ_p the stripping radii increase, as witnessed

by the third, ground, and first excited states having $\ell_p = 2, 1, 0$ and $r_p = 5.5, 5.3,$ and 3.6 fermis, respectively.

b. Distorted Wave Analysis

The excited states of N^{13} are unbound to proton emission and therefore could not be analyzed by an available distorted wave code. This analysis was therefore confined to the ground state. The only distorted wave analysis of this state was done by Hodgson (Ho 63) and by Smith (Sm 63) with the 1.45 to 2.95 MeV data of Elwyn, Kane, and Ofer (El 59). Optical potential parameters were chosen consistent with those found in that work. The code was one written by Smith (Sm 65) and previously adapted for the University of Alberta IBM 7040 computer. The optical potentials chosen were of the form

$$U(r) = V_c(r) - V_o f_{ws}(r,R,a) - i4aW_o \frac{d}{dr} f_{ws}(r,R,a) \qquad \text{(IV-1)}$$

where $f_{ws}(r,R,a) = 1/(1 = \exp((r - r_o A^{1/3})/a))$

and $V_c(r)$ is the Coulomb potential due to a uniformly charged sphere. r is the relative separation of the reacting nuclei, r_o and a are the radius and diffuseness parameters respectively for the Woods-Saxon form factor; V_o and W_o are the strengths of the refracting and surface absorbing parts of the optical potential. The factor 4 gives the surface form factor unity for its maximum value. The program approximates the finite range n-p interaction, the nonlocality of the potential, and the deuteron polarizability.

The parameter values are given in Figure 4-3. Table IV-1 presents a list of the optical potential parameters used for deuterons on C^{12}. σ_R is the reaction cross section and was extracted where not given and for the present experiment from the elastic search code of Perey. The apparent violation of the Vr^n ambiguity in the two sets of parameters in the present experiment is probably due to the fact that for deuterons there are discrete sets of V_o for a given r_o which provide equally good fits to the data (Pe 63, Dr 63).

The need for a spin-orbit term in the incoming and outgoing channels is evident from the too high theoretical distributions at back angles (Sh 62).† Inspection of Table IV-1 reveals a real potential approximately constant with bombarding energy and an imaginary term increasing with bombarding energy. This behaviour is consistent with the investigation of Perey and Dickens (Pe 65). They find that the real term is a slowly decreasing function of energy while the variation of the imaginary term with energy is sensitive to the absolute data normalization. However the startling agreement with the parameters of Smith's (Sm 63) 2.75 MeV analysis suggests that the

---

† Write the scattering amplitude as a sum of a unit matrix and the Pauli spin matrices (for spin 1/2). Then compare the two ratios $d\sigma(\pi)/d\sigma(\theta) = |a(\pi)|^2/|a(\theta)|^2$ with no spin-orbit term and $d\sigma(\pi)/d\sigma(\theta) = |a(\pi)|^2/[|a(\theta)|^2 + |b(\theta)|^2\sin^2\theta]$ with an $\underline{\ell}\cdot\underline{s}$ term, where $0 \leq \theta \leq \pi$.

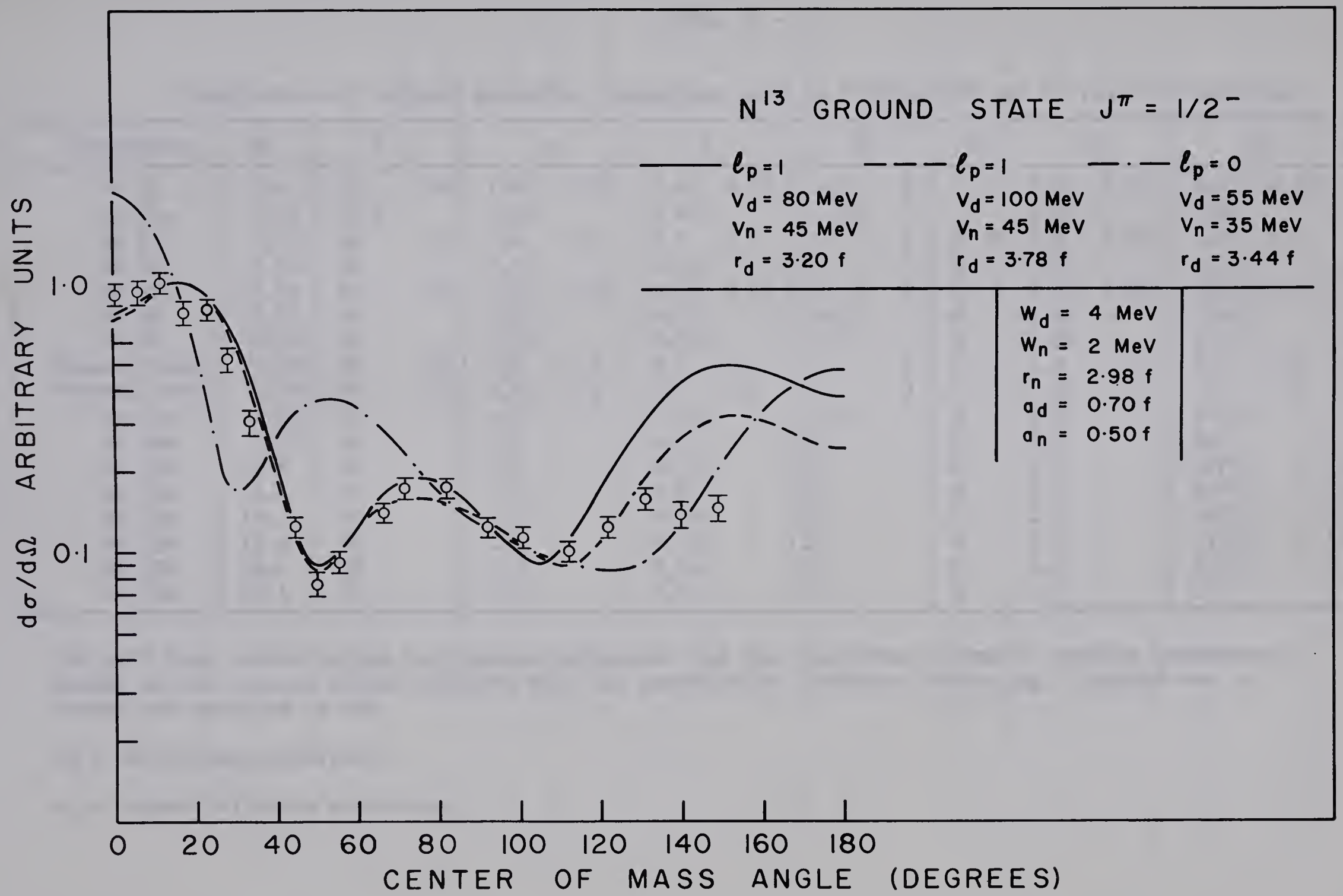

FIGURE 4-3· ANGULAR DISTRIBUTION FROM $C^{12}(d,n)N^{13}$ LEADING TO THE GROUND STATE OF N^{13}· DISTORTED WAVE PREDICTIONS ARE SHOWN·

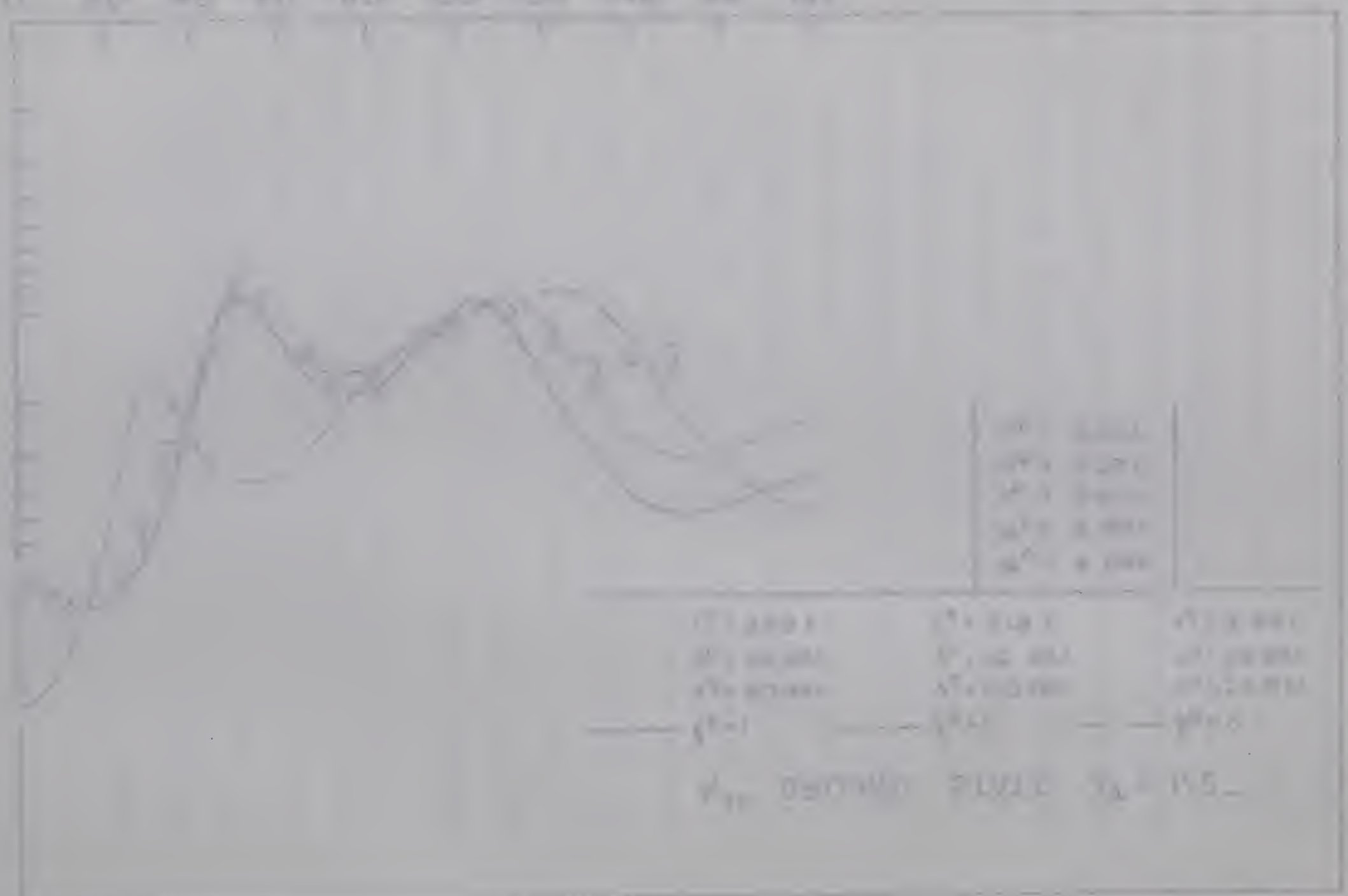

TABLE IV - 1

Compilation of optical potential parameters used in $^{12}C(d,n)^{13}N$ and $^{12}C(d,d)^{12}C$ analyses

Reference	E_D	U		r_o		a		W_S		W_D		r'_o		a'		σ_R(mb)
Ho 63	1.6	63	45	1.45	1.25	0.65	0.65	0.5	8	0	0	1.45	1.25	0.65	0.65	113
Ho 63a	1.72	53.2		1.35		0.64		1.52				1.35		0.64		170
Sm 63	2.75	80	51	1.4	1.25	0.7	0.5	4	2	0	0	1.4	1.25	0.7	0.5	697
Wi 66	2.80	30		2.57		0.31		35		0		0.40		1.25		1097
Ho 63	2.85	63	45	1.45	1.25	0.65	0.65	2	3	0	0	1.45	1.25	0.65	0.65	410
Wi 66	3.23	60		1.67		0.57		9.0		0		1.49		0.41		920
Wi 66	3.70	56		1.80		0.53		5.7		0		1.97		0.14		1001
Present Work	5.994	80	45	1.4	1.3	0.7	0.5	0	0	4	2	1.4	1.3	0.7	0.5	961
Present Work	5.994	100	45	1.65	1.3	0.7	0.5	0	0	4	2	1.65	1.3	0.7	0.5	1096
Ho 63a	7.86	32		1.5		0.53		6.5		0		1.5		0.53		772
Ho 63a	7.86	70		1.5		0.6		11		0		1.5		0.6		990
Ho 63a	11.8	60		1.5		0.79		11		0		1.5		0.79		1210
Ho 63a	13.0	50		1.5		0.81		19		0		1.5		0.81		1260
Ho 63a	14.7	50		1.5		0.79		16		0		1.5		0.79		1180
Ho 63a	15.9	50		1.5		0.73		15		0		1.5		0.73		1090
Ho 63a	18.1	50		1.5		0.66		15		0		1.5		0.66		970
Ho 63a	28.1	60		1.5		0.6		15		0		1.5		0.6		860

The left hand column refers to deuteron parameters and the right hand column to neutron parameters. Blanks in the neutron column indicate that the reaction was deuteron scattering. Lengths are in fermis and energies in MeV.

W_S = Woods-Saxon absorption.

W_D = Saxon-derivative absorption.

potentials are also sensitive to the code used.

c. J-Dependence of the Angular Distribution of the 3.51 MeV State ($J^\pi = 3/2^-$) and Ground State ($J^\pi = 1/2^-$) of N^{13}

Lee and Schiffer (Le 64) observed that (d,p) angular distributions with $\ell_n = 1$ neutrons populating $J = 1/2$ states exhibit deep minima sometimes at about 100° but most often at about 130°. This survey was limited to mass number $40 < A < 65$ and energy $7 \leq E_D \leq 12$ MeV. Recently Davies et al. (Da 66) found a similar behaviour still perceptible at 5 MeV for the $Si^{28}(d,n)P^{29}$ reaction leading to the first and second excited states of P^{29}, $\ell_p = 2$.

The ground state ($J^\pi = 1/2^-$) and 3.51 MeV state ($J^\pi = 3/2^-$) angular distribution are shown in Figure 4-4. The apparent absence of the Lee-Schiffer effect in this experiment should be considered with caution due to the large error in the angular distribution for the second excited state of N^{13}. It is possible to conclude, nevertheless, that J dependence is probably absent at this energy for this nucleus. This is indicated by the smoothness of the large angle distribution for the ground state group. The sparse data at higher energies shows a fairly uniform large angle ground state distribution as well (Ko 63).

A large angle comparison of the corresponding mirror states in C^{13} is not available. The $C^{12}(d,n)C^{13}$ ground state angular distribution is uniform between 7 and 11 MeV (Ev 63) with a dip at 11 MeV and 90 degrees. Schmidt-Rohr et al. (Sc 63) however find that the

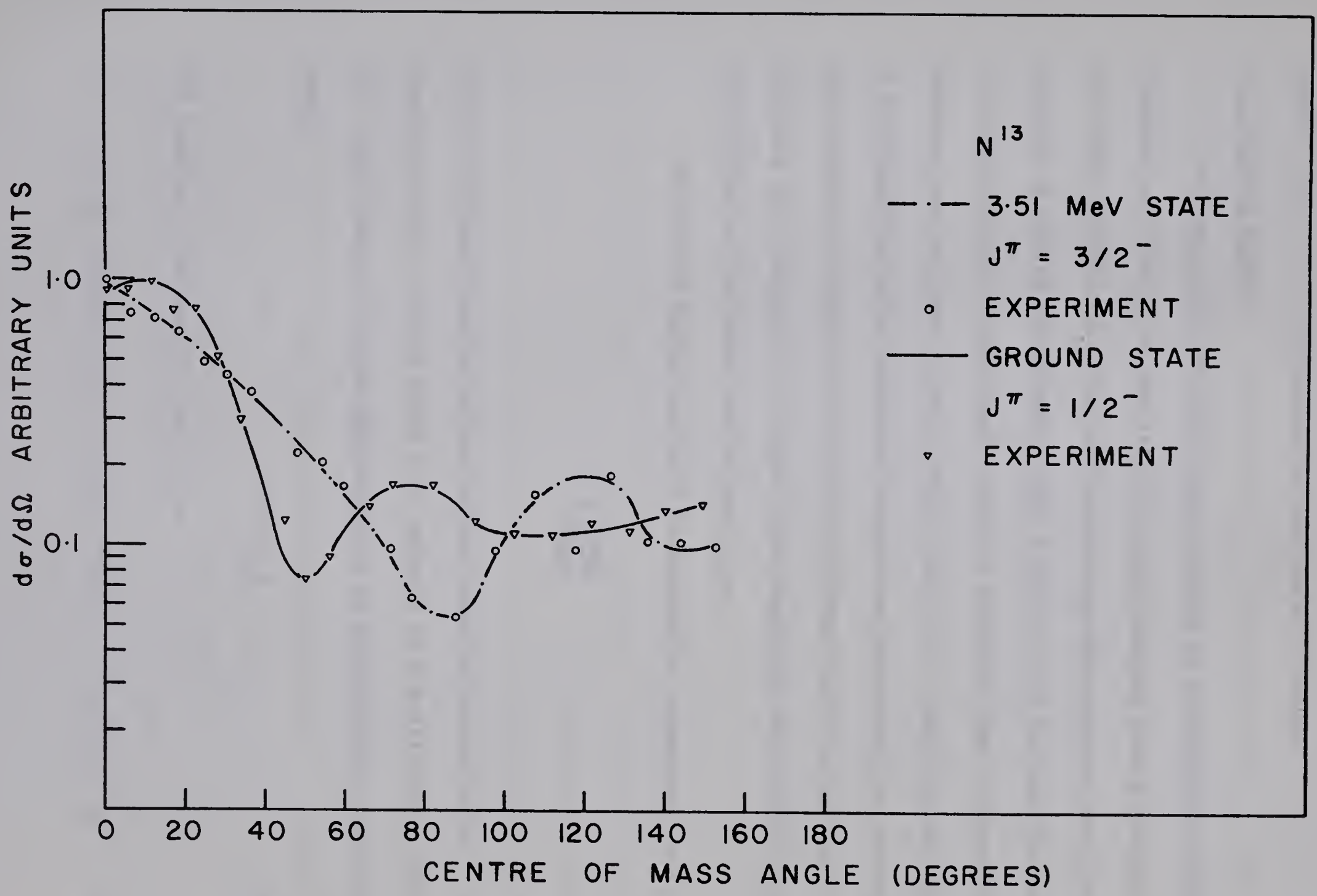

FIGURE 4-4· ANGULAR DISTRIBUTION OF THE GROUND STATE VERSUS THE 3·51 MEV STATE OF N^{13}· THE SMOOTH CURVES ARE DRAWN THROUGH THE DATA TO SHOW STRUCTURE IN THE ANGULAR DISTRIBUTIONS

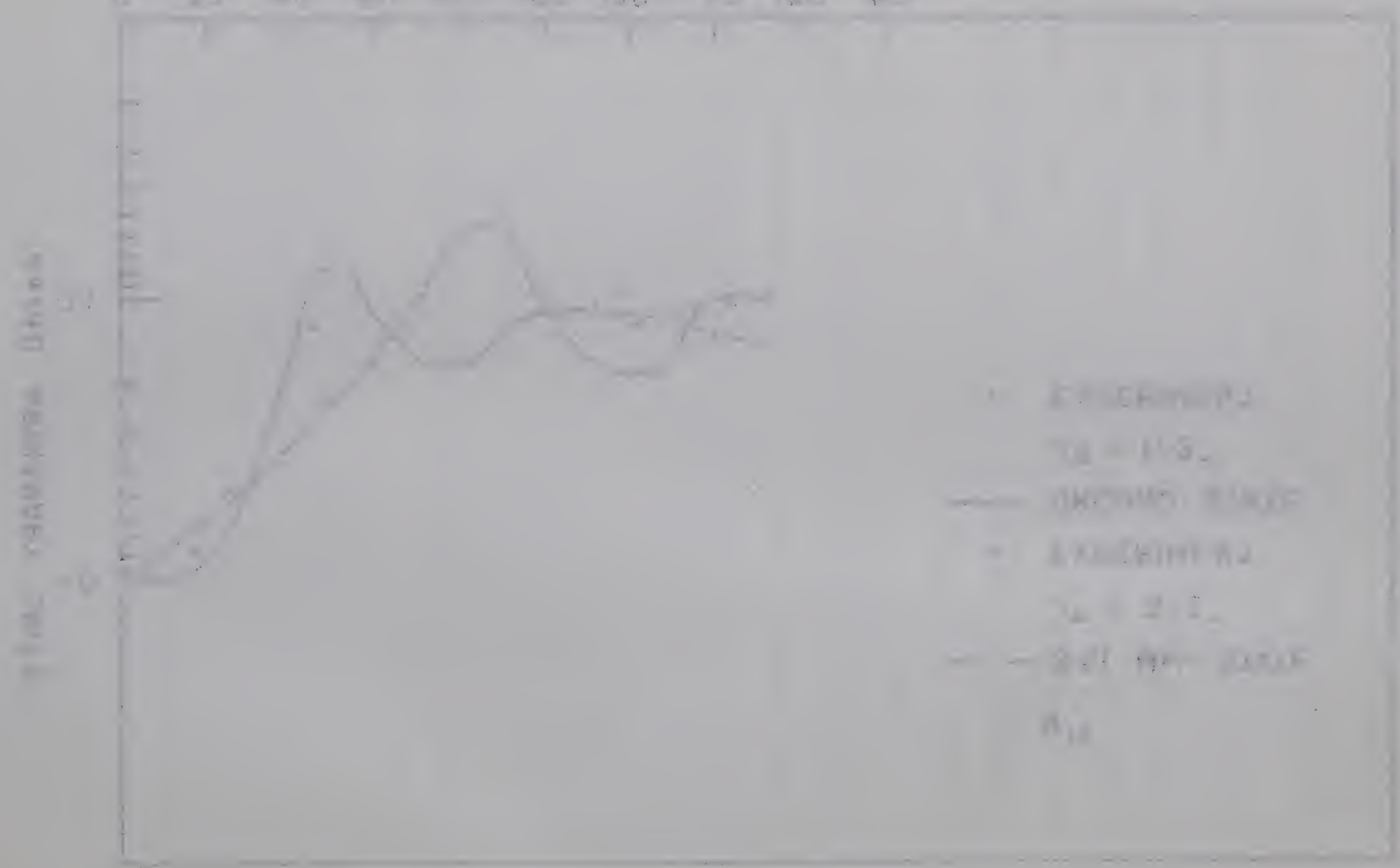

ground state C^{13} distribution is uniform at 11.8 MeV.

d. Reduced Widths

The expression for the cross section in a stripping reaction contains an overlap of the initial target nucleus wave function with the final nuclear wave function containing the captured particle. This overlap is called the spectroscopic factor S. If the stripped nucleon is captured into a pure single particle state so that the passive nucleons are in their initial state then S = 1. How well we can deduce S by comparison with experiment depends on how exactly we can express the remaining integral in the expression for the cross section. This contains the overlap of the three wave functions describing the relative motion of the three active particles.

In the DWB approximation S is related to experiment by

$$S = \frac{\sigma_{exp}}{\sigma_{DWB}} \qquad \text{(IV-2)}$$

In the PWB approximation with a radial cutoff a second factor, the single particle reduced width θ_o^2, appears as a multiplying factor. The cross section in this approximation is proportional to the reduced width

$$\theta^2 = S\theta_o^2 \qquad \text{(IV-3)}$$

The general relationship (Bu 61) is

$$S^{1/2} \simeq \sum_{j\ell} \theta_{j\ell} \langle J_t j M_t m | J_r M_r \rangle \langle \ell s \lambda \mu | j m \rangle \cdot R_\ell(r_p) \; i^\ell Y_\ell^m(\underline{r}_p) \; {}^*\chi_s^{\mu *} \qquad \text{(IV-4)}$$

Reduced widths were extracted in the present experiment and are tabulated in Table IV-2. Plane wave reduced widths were calculated using formula (A-17) of French (Fr 60). The value found in this experiment for the ground and 3.56 MeV state agree qualitatively with those found at neighboring energies. The singularity of the theory for the 2.367 MeV state is clearly evident in the large fluctuations of the reduced widths for that state. The relatively low ground state value suggests that the target might be thinner to the beam than measured. Agreement of the plane wave spectroscopic factors with those from the distorted wave calculation would require a single particle reduced width different from those found by MacFarlane and French (Ma 60) for C^{13} by a factor of five. This is in agreement with the greater reliability of the DWB calculation.

The DWB calculation was carried out with a program using j-j coupling wave functions for the final nucleus. j-j coupling in fact seems to be the better choice for 1p shell nuclei above mass 10 (La 53), although neither extreme coupling scheme gives as good agreement with the level structure as intermediate coupling (ibid., Co 65).

e. Conclusion

The present experiment could not sufficiently separate the doublet in N^{13} to present an unambiguous comparison of the ground and second excited states. We can however accept the absence of the Lee-Schiffer dip as evidence for the lack of J dependence. This is supported by the lack of structure in the ground state of C^{13} between

TABLE IV - 2

Spectroscopic factors for the mirror nuclei ^{13}N - ^{13}C h)

E_x (J^π_f)	r_o PWBA	E_D	θ^2_{abs}	S_{abs} DWBA	S_{rel} PWBA	S_{rel} DWBA	Calc Rel c)
3.56 ($\frac{5^+}{2}$)	5.5	5.994 a)	0.033		2.04		
	5.5	5.994 b)	0.02		1.25		
		9 c)			3.47		
	5.0		0.072		2.29		
							7.83
3.51 ($\frac{3^-}{2}$)	3.5	5.994 b)	0.006		0.35		
	7.5	5.994 b,e)	0.008		0.31		
2.367 ($\frac{1^+}{2}$)	3.6	5.994	0.114		7.12		
	6	5.994 e)	0.0077		0.30		
	8	13.0	0.064 d)		2.06		
							25.2
0 ($\frac{1^-}{2}$)	4.7	2.68	0.024		1	1	
	4.7	3.26	0.021		1	1	
	5.3	5.994	0.016	1.56 f)	1	1	
	6.0	5.994 e)	0.026	2.20 g)	1	1	
	4.5	9	0.047		1	1	
	4.5	13	0.031 d)		1	1	

E_x (J^π_f)	r_o	E_D	θ^2_{abs} PWBA	S_{abs} DWBA	S_{rel} PWBA	S_{rel} DWBA	Calc i) Rel
3.85 ($\frac{5^+}{2}$)		2.8	0.022	2.2			1.17
		3.23	0.027	1.03			2.0
		3.70	0.046	1.27			
	4.2	8.0	0.098		1.7		
	4.5	9.0	0.073		1.8		
	5.4	14.8	0.071		2.3		
3.68 ($\frac{3^-}{2}$)		2.80	0.0027	0.19			0.32
		3.23	0.0063	0.23			0.37
		3.70	0.0056	0.17			
	4.2	8.0	0.006		0.1		
	4.5	9.0	0.013		0.31		
	4.0	14.8	0.006		0.19		
3.09 ($\frac{1^+}{2}$)	4.2	8	0.18		3.1		5.4
	4.5	9	0.19		4.6		2.9
	4.0	14.8	0.15		4.9		
0 ($\frac{1^-}{2}$)	7.1	2.68	0.022		1		1
	6.15	3.29	0.025		1		1
	4.2	8	0.056		1		
	4.5	9	0.042				
	4.0	14.8	0.031				

a) unseparated
b) separated
c) ref. Ca 57
d) ref. Wi 66
e) Z = 6 in PWBA
f) V_D = 80 MeV, r_{OD} = 1.4 fm
g) V_D = 100 MeV, r_{OD} = 1.65 fm
h) ref. Ma 60, Ge 66
i) ref. Ca 57, not at the corresponding energy

Lengths in fermis and energies in MeV

7 and 11 MeV (Ev 63, Sc 63). It would be worthwhile doing the $C^{12}(d,p)C^{13}$ reaction in the 6 MeV range as there the doublet in C^{13} should be readily resolved.

Bassel (Ba 62) points out that the cross section can be written as the sum of two terms

$$\frac{d\sigma}{d\Omega} = A(\theta) + (-1)^{J-\ell-1/2}B(\theta) \qquad \text{(IV-1)}$$

with $A(\theta)$ arising from the central well distortions and $B(\theta)$ proportional to the spin-orbit strengths of the optical wells. In view of the conclusion concerning the distorted wave fits in section IV b. at back angles, J dependence does not seem to stem solely from the spin orbit wells as these are necessary to suppress the back angle rise in the theoretical distribution.

APPENDIX

a. General Derivation of the (d,n) Cross Section

In a (d,n) reaction, ignoring center of mass motion, the Hamiltonian of the colliding system can be written in terms of final coordinates (Mo 65) as

$$H(\underline{r}_p,\underline{r}_n,\xi) = K(\underline{r}_n) + H_F(\underline{r}_p,\xi) + V_{nI}(\underline{r}_n',\xi) + V_{np}(|\underline{r}_n' - \underline{r}_p|) \qquad (A\text{-}1)$$

where $K(\underline{r}_n) = -(\hbar^2/2M_F)\nabla_n^2$ is the kinetic energy of relative motion, H_F is the Hamiltonian of the final nucleus, V_{nI} is the interaction of the neutron with the nucleons of the target nucleus and V_{np} that with the captured proton. $\underline{r}_p$ and $\underline{r}_n'$ are the coordinates of the captured proton and of the ejected neutron relative to the c. of m. of the initial nucleus, $\underline{r}_n$ that of the ejected neutron relative to the c. of m. of the final nucleus. Thus $\underline{r}_n' = \underline{r}_n + [m/(m + M_T)]\underline{r}_p$. M_F is the reduced mass for the motion of the neutron relative to the final nucleus. M_T and m are the target and proton masses, respectively. The corresponding time independent Schroedinger equation for the system is

$$H(\underline{r}_p, \underline{r}_n,\xi)\Psi(\underline{r}_p, \underline{r}_n,\xi) = E\Psi(\underline{r}_p,\underline{r}_n,\xi) \qquad (A\text{-}2)$$

We next expand Ψ in the form

$$\Psi(\underline{r}_p,\underline{r}_n,\xi) = \sum_s \phi_s(\underline{r}_p,\xi)G_s(\underline{r}_n) \qquad (A-3)$$

where ϕ_s is the wave function for the s^{th} state of the final nucleus of energy ε_s, so that

$$H_F(\underline{r}_p,\xi)\phi_s(\underline{r}_p,\xi) = \varepsilon_s\phi_s(\underline{r}_p,\xi) \qquad (A-4)$$

and ϕ_s, G_s are assumed to be complete in s.

Using relations (A-1) and (A-3), (A-2) becomes

$$\left(K(\underline{r}_n) + H_F(\underline{r}_n,\xi) + V_{nI}(\underline{r}_n',\xi) + V_{np}(|\underline{r}_n' - \underline{r}_p|)\right)\sum_s \phi_s(\underline{r}_p,\xi)G_s(\underline{r}_n)$$

$$= E\sum_s \phi_s(\underline{r}_p,\xi)G_s(\underline{r}_n) \qquad (A-5)$$

Multiplying by ϕ_t^* and integrating over the coordinates $(\underline{r}_p,\xi)$ yields

$$\left(K(\underline{r}_n) + \varepsilon_t\right)G_t(\underline{r}_n) + \sum_s \int\int d\underline{r}_p d\xi \phi_t^*(\underline{r}_n,\xi)[V_{nI}(\underline{r}_n',\xi)$$

$$+ V_{np}(|\underline{r}_n' - \underline{r}_p|)]\phi_s(\underline{r}_p,\xi)G_s(\underline{r}_n) = EG_t(\underline{r}_n)$$

or
$$-\left(K(\underline{r}_n) - (E - \varepsilon_t)\right)G_t(\underline{r}_n) = \sum_s V_{ts}(\underline{r}_n')G_s(\underline{r}_n) \qquad (A-6)$$

where $E - \varepsilon_t$ is the energy of relative motion and

$$V_{ts}(\underline{r}_n') = \int d\underline{r}_p d\xi \phi_t^*(\underline{r}_p,\xi)[V_{nI}(\underline{r}_n',\xi) + V_{np}(|\underline{r}_n' - \underline{r}_p|)]\phi_s(\underline{r}_p,\xi) \qquad (A-7)$$

Equation (A-6) represents a set of coupled equations for the wave function $G_k(\underline{r}_n)$ of the relative motion in terms of the set $\phi_k(\underline{r}_p,\xi)$, which describe the states of the final nucleus, and the

potential $\left(V_{nI}(\underline{r}_n',\xi) + V_{np}(|\underline{r}_n' - \underline{r}_p|)\right)$. Writing out in full and rearranging slightly gives

$$-\left(K(\underline{r}_n) - (E - \varepsilon_o) + V_{oo}(\underline{r}_n')\right)G_o(\underline{r}_n) = 0 + V_{01}(\underline{r}_n')G_1(\underline{r}_n) + \ldots$$

$$-\left(K(\underline{r}_n) - (E - \varepsilon_1) + V_{11}(\underline{r}_n')\right)G_1(\underline{r}_n) = V_{10}(\underline{r}_n')G_o(\underline{r}_n) + 0 + \ldots \qquad \text{(A-8)}$$

$$\vdots \qquad \vdots \qquad \vdots \qquad \vdots$$

The set of equations (A-8) is general but prohibitively complicated. Neglect of antisymmetrization with respect to the exchange of identical particles plus the following approximations may be accounted for by slight variation of the imaginary terms of the optical potentials.

In a (d,n) reaction populating one state k only, the set (A-8) reduces to

$$-\left(K(\underline{r}_n) - (E - \varepsilon_o) + V_{oo}(\underline{r}_n')\right)G_o(\underline{r}_n) = V_{ok}(\underline{r}_n')G_k(\underline{r}_n)$$

$$-\left(K(\underline{r}_n) - (E - \varepsilon_k) + V_{kk}(\underline{r}_n')\right)G_k(\underline{r}_n) = V_{ko}(\underline{r}_n')G_o(\underline{r}_n) \qquad \text{(A-9)}$$

This is the two state coupled channels approximation.

In the next approximation the advantage of rearrangement collisions over inelastic scattering will become evident. This is due to the fact that in inelastic scattering, the elastic channel is always dominant while in rearrangement there is no source of elasti-

cally scattered outgoing particles. I.e. in rearrangement collisions $V_{ok}G_k >> V_{ko}G_o$ while the reverse inequality holds true in inelastic scattering. In this approximation we get a pair of uncoupled equations

$$-\left(K(\underline{r}_n) - (E - \varepsilon_o) + V_{oo}(\underline{r}_n')\right)G_o(\underline{r}_n) = V_{ok}(\underline{r}_n')G_k(\underline{r}_n)$$

$$\left(K(\underline{r}_n) - (E - \varepsilon_k) + V_{kk}(\underline{r}_n')\right)G_o(\underline{r}_n) = 0 \qquad \text{(A-10)}$$

Equation (A-10a) reads

$$-\left(K(\underline{r}_n) - (E - \varepsilon_o) + V_{oo}(\underline{r}_n')\right)G_o(\underline{r}_n) \qquad \text{(A-11)}$$

$$= \int\int d\underline{r}_p d\xi \phi_o^*(\underline{r}_n,\xi)[V_{nI}(\underline{r}_n',\xi) + V_{np}(|\underline{r}_n' - \underline{r}_p|)]\phi_k(\underline{r}_p,\xi)G_k(\underline{r}_n)$$

Since now our expansion for $\Psi(\underline{r}_p,\underline{r}_n,\xi)$, equation (A-3), contains only one term, the k^{th} term, we can equate $\phi_k(\underline{r}_p,\xi)G_k(\underline{r}_n)$ in equation (A-11) to the incident wave.

$$F_o(\underline{r}_d)\chi(|\underline{r}_n' - \underline{r}_p|)\psi_I(\xi) \qquad \text{(A-12)}$$

F_o is the wave function for the deuteron motion relative to the initial nucleus, χ is the deuteron wave function, ψ_I is the wave function of the ground state of the target nucleus; and $\underline{r}_d = (\underline{r}_n' + \underline{r}_p)/2$. χ is not to be confused with the spin functions of equation IV-4. F_o is a solution of

$$[K(\underline{r}_d) - (E - e_o) + V_{oo}(\underline{r}_d)]F_o(\underline{r}_d) = 0 \qquad \text{(A-13)}$$

where $e_o = 0$ and

$$V_{oo}(\underline{r}_d) = V_{dI}(\underline{r}_d) \tag{A-14}$$

F_o is subject to the boundary condition

$$F_o(\underline{r}_d) \xrightarrow[r_d \to \infty]{} e^{i\underline{k}_d \cdot \underline{r}_d} + \frac{M_I}{2\pi\hbar^2} \frac{e^{ik_d r_d}}{r_d} f(\theta_d, \phi_d)$$

(A-11) then becomes

$$-\left(K(\underline{r}_n) - (E - \varepsilon_o) + V_{oo}(\underline{r}_n')\right)G_o(\underline{r}_n) =$$

$$\int\int d\underline{r}_p d\xi \phi_o^*(\underline{r}_p, \xi)[V_{nI}(\underline{r}_n', \xi) + V_{np}(|\underline{r}_n' - \underline{r}_p|)]\psi_I(\xi)\chi(|\underline{r}_n' - \underline{r}_p|)$$

$$\times F_o(\underline{r}_d) \tag{A-15}$$

$G_o(\underline{r}_n)$ can now be solved for subject to the boundary condition

$$G_o(\underline{r}_n) \xrightarrow[r_n \to \infty]{} \frac{M_F}{2\pi\hbar^2} \frac{e^{ik_n r_n}}{r_n} g(\theta, \phi) \tag{A-16}$$

where $k_m^2 = \frac{2M_m}{h^2}(E - \varepsilon_m)$, M_m is the reduced mass in channel m, and

$g(\theta,\phi)$ is the transition amplitude for the channel m. The solution of (A-15) can be arrived at using the Green's function method. First the right hand side of (A-15) is set equal to zero to yield a homogeneous equation having the same form as the optical model problem. Hence V_{oo} can be found from neutron scattering at the energy E. In

inelastic scattering we would have to extract V_{kk} from (A-9b). It is impractical to observing elastic scattering from excited nuclei, although scattering with energy $(E - \varepsilon_k)$ is sufficient. At any rate V_{oo} is often used.

The Green's function for (A-15) can be written in terms of $\overline{G}_o(\underline{r}_n,\theta)$ where

$$\left(K(\underline{r}_n) - (E - \varepsilon_o) + V_{oo}(\underline{r}_n')\right)\overline{G}_o(\underline{r}_n,\theta) = 0 \qquad \text{(A-17)}$$

satisfying

$$\overline{G}_o(\underline{r}_n,\theta) \xrightarrow[r_n \to \infty]{} e^{i\underline{k}_n\cdot\underline{r}_n} + \frac{M_F}{2\pi\hbar^2}\,\frac{e^{ik_n r_n}}{r_n}\,g(\theta,\phi) \qquad \text{(A-18)}$$

Then

$$G_o(\underline{r}_n) = \frac{M_F}{2\pi\hbar^2}\,\frac{e^{ik_n r_n}}{r_n}\iiint d\underline{r}_p d\underline{r}_n d\xi \overline{G}_o(\underline{r}_n,\pi-\Theta)\phi_o^*(\underline{r}_p,\xi)$$

$$\times\,[V_{nI}(\underline{r}_n',\xi) + V_{np}(|\underline{r}_n' - \underline{r}_p|)]\psi_I(\xi)\chi(|\underline{r}_n' - \underline{r}_p|)F_o(\underline{r}_d) \qquad \text{(A-19)}$$

where

$$\cos\Theta = \cos\theta\cos\theta_n + \sin\theta\sin\theta_n\cos(\phi - \phi_n) \qquad \text{(A-20)}$$

At this point it is usual to neglect $V_{nI}(\underline{r}_n',\xi)$. One justification for this is to write

$$\phi_k(\underline{r}_p,\xi) = \psi_c(\xi)\omega_k(\underline{r}_p) \qquad \text{(A-21)}$$

in equation (A-11) and make use of the orthogonality property of the

ω_k. Comparison of (A-16) with (A-19) then yields

$$g(\theta,\phi) = \iiint d\underline{r}_p d\underline{r}_n d\xi \bar{G}_o(r_n,\pi-\theta)\phi_o^*(\underline{r}_p,\xi)$$

$$\times V_{np}(|\underline{r}_n' - \underline{r}_p|)\psi_I(\xi)\chi(|\underline{r}_n' - \underline{r}_p|)F_o(\underline{r}_d) \qquad \text{(A-22)}$$

and

$$\frac{d\sigma}{d\Omega} = \frac{M_I M_F}{(2\pi\hbar^2)^2}\frac{k_n}{k_d}\left|g(\theta,\phi)\right|^2 \qquad \text{(A-23)}$$

In the foregoing, spins have been neglected for clarity. In the plane wave Born approximation the diagonal terms $V_{oo}(\underline{r}_d)$ and $V_{oo}(\underline{r}_n)$, i.e. the optical plus Coulomb potentials, are set equal to zero.

b. Programs

In the light of the above discussion it was felt necessary to be able to readily derive the potentials from elastic scattering. The recently operational magnetic spectrometer at the University of Alberta in fact provides a useful tool for this.

Two elastic search codes were subsequently converted for running on the University of Alberta IBM 7040. These are Perey's code and the code SEEK by Melkanoff (Bu 60, Bu 61, Ma 62, Me 65, Me 66, Ma 66). The cross sections are found from the scattering coefficients C_ℓ which in turn are solutions of

$$f_\ell = \left(\frac{F_\ell'(\rho) + iG_\ell'(\rho) + C_\ell[F'(\rho) - iG_\ell'(\rho)]}{F_\ell(\rho) + iG(\rho) + C_\ell[F_\ell(\rho) - iG_\ell(\rho)]}\right)_{\rho = \rho_M}$$

f_ℓ is the logarithmic derivative determined from the internal integra-

tion. $F_\ell(\rho)$ and $G_\ell(\rho)$ are the regular and irregular Coulomb wave functions.

Perey's code uses the Cowell or Fox-Goodwin method (Fo 49, Me 65, Bu 62) for the internal integration. For the search the function

$$\chi^2 = F(\underline{p}) = \sum_\lambda [(f_\lambda(\underline{p}) - f_\lambda^*)/\Delta f_\lambda^*]^2 \qquad \text{(A-25)}$$

of the n search parameters $p_1, p_2, \ldots p_n$ generates a true χ^2 surface. f_λ and f_λ^* are theoretical and experimental quantities, respectively. The true χ^2- surface is approximated by a quadratic χ^2- surface defined by

$$\chi^2 = \overline{F}(\underline{p}) \qquad \text{(A-26)}$$

where $\overline{F}(\underline{p})$ is obtained by a second order Taylor expansion of $F(\underline{p})$ around the central point $\underline{p}^\circ$

$$\overline{F}(\underline{p}) = F(\underline{p}^\circ) + \sum_i \frac{2F}{2p_i}\Bigg|_{\underline{p}^\circ} \delta p_i + \frac{1}{2} \sum_{i,j} \frac{\partial^2 F}{\partial p_i \partial p_i}\Bigg|_{\underline{p}^\circ} \delta p_i \delta p_j \qquad \text{(A-27)}$$

and

$$\underline{p} = \underline{p}^\circ + \delta\underline{p} \qquad \text{(A-28)}$$

In a neighborhood of $\underline{p}^\circ$ the $f_\lambda(\underline{p})$ are approximated by the first order Taylor series

$$f_\lambda(\underline{p}) = f_\lambda(\underline{p}^\circ) + \sum_\lambda \frac{\partial f_\lambda}{\partial p_i}\Bigg|_{\underline{p}^\circ} \delta p_i \qquad \text{(A-29)}$$

Partial derivatives of F are given by

$$\left.\frac{\partial F}{\partial p_i}\right|_{\underline{p}^\circ} = 2\sum_\lambda \frac{(f_\lambda(\underline{p}^\circ) - f_\lambda^*)}{(\Delta f_\lambda^*)^2} \left.\frac{\partial f_\lambda}{\partial p_i}\right|_{\underline{p}^\circ} \tag{A-30}$$

$$\left.\frac{\partial^2 F}{\partial p_i \partial p_j}\right|_{\underline{p}^\circ} = 2\sum_\lambda \frac{1}{(\Delta f_\lambda^*)^2} \left.\frac{\partial f_\lambda}{\partial p_i}\right|_{\underline{p}^\circ} \left.\frac{\partial f_\lambda}{\partial p_j}\right|_{\underline{p}^\circ} \tag{A-31}$$

Substitution of eqs. (A-30) and (A-31) into eq. (A-27) yields the quadratic χ^2 surface $\chi^2 = \overline{F}(\underline{p})$. Contributions from second partial derivatives of f_λ are neglected in eq. (A-31). The first order partial derivatives of f_λ are approximated by difference quotients

$$\left.\frac{\partial f_\lambda}{\partial p_i}\right|_{p^\circ} \simeq \frac{f_\lambda(p_i^\circ + \Delta p_i) - f_\lambda(p_i^\circ - \Delta p_i)}{2\Delta p_i}$$

requiring n + 1 runs at $\underline{p}^\circ$ and $(p^\circ_1, \circ\circ\circ, p_i{}^\circ_{-1}, p_i{}^\circ + \Delta p_i, p_i{}^\circ_{+1}, \circ\circ\circ, p_n{}^\circ)$ for all i.

Descent and termination proceed by the relation

$$\left.\frac{\partial \overline{F}}{\partial p_i}\right|_{\underline{p}} = \left.\frac{\partial F}{\partial p_i}\right|_{\underline{p}^\circ} + \sum_{j=1}^{n} \left.\frac{\partial^2 F}{\partial p_i \partial p_j}\right|_{\underline{p}^\circ} \delta p_j = 0 \quad (i = 1, \circ\circ\circ, n) \tag{A-33}$$

at the minimum. The solution of this system of linear equation for $\delta\underline{p}$ yields the predicted minimum point

$$\underline{p} = \underline{p}^\circ + \delta\underline{p} \tag{A-28}$$

The further $\underline{p}$ is from $\underline{p}^\circ$ the less reliable is the prediction of a χ^2

minimum. Proportionately smaller steps than $\delta\underline{p}$ are then taken empirically. A parabolic approximation with two neighboring values of $\underline{p}$ is used to choose the next central point. The total number of runs required per central guess is n + 3. A sufficiently small improvement in χ^2 from one central point to the next central point terminates the search.

The code SEEK uses the modified Noumerov (Me 65) integration method for the internal solution. This is an extension of the Fox-Goodwin method requiring less computation and no division. The exploration phase of the search is the same as that in Perey's code except that the first order partial derivatives of f_λ are calculated analytically using the formula (Me 64)

$$\frac{\partial C_\ell}{\partial p_i} = -\frac{1}{E}\frac{1}{(\alpha_\ell)^2}\int_0^{\rho_m}(\psi_\ell)^2\,\frac{\partial V_\ell}{\partial p_i}\,d\rho \qquad (A\text{-}34)$$

α_ℓ is a normalization constant and

$$V_\ell = V_{coul} + V_{cR} + iV_{cI} + V_{sR} + iV_{sI} \qquad (A\text{-}35)$$

These are the Coulomb, complex central and complex spin-orbit potentials, respectively. The derivatives of the cross sections in turn are directly related to $\partial C_\ell/\partial p_i$. This method of obtaining the quadratic surface requires only one run and several numerical integrations as indicated by eq. (A-34) per central guess. This compares favourably with the n + 3 runs required by the Oak Ridge method. Both

codes require the inversion of a p × p matrix at each central point as indicated by equation (A-33).

Perey's code was modified to accomodate a grid variation over the starting values of the parameters. Deuteron polarizability and non-locality was included for compatability with Smith's DW (Sm 65, Di 65) code. Deuteron polarizability is due to the displacement of the charge of the deuteron from its center of mass and may be accounted for by an attractive dipole potential

$$-\frac{1}{2}\frac{Z^2e^4\alpha}{r^4} \qquad \text{(A-36)}$$

external to the nuclear field. Z is the charge of the target nucleus. Dickens and Perey (Di 65) use $\alpha = 0.5$ (fermis)^3 while Smith (Sm 65) uses $\alpha = 0.445$ (fermis)^3.

Nonlocality, which means that the wave function at r is affected by its value at r', can be approximated (Ba 62, Sm 65) by

$$\psi_{NL}(r) = [1 + \frac{\beta^2}{4} U(r)]^{-1/2} \psi_L(r) \qquad \text{(A-37)}$$

where $U(r) = 2mV(r)/h^2$ is the real part of the potential. The non-locality range β is usually 0.85 fermis.

Table (A-1) lists the imput format to Perey's code. The potential is of the form

$$U(r,\sigma) = V_c(r,R_c) - V_o f_{ws}(r,R_R,a_R) - cW_s f_{ws}(r,R_I,a_I) \qquad \text{(A-38)}$$

$$- i4a_I W_D \frac{d}{dr} f_{ws}(r,R_I,a_I) - \underline{\ell}\cdot\underline{\sigma}(V_{so} + iW_{so})\left(\frac{h}{2m_pc}\right)^2 \frac{1}{r}\frac{d}{dr} f_{ws}(r,R_R,a_R)$$

TABLE A - 1

Card Set	Symbol	Definition	Format
1	I7	Function control	(I2,I8, 2F10.3,50H ....)
	NORM	If ≠0, the first NORM points are used to search for the best normalization.	
	WNCUM	If ≠0, all experimental cross sections and errors are multiplied by WNCUM before calculation is started.	
	ERN	If ≠0, the renormalization by NORM is constrained from varying too far from unity. ERN may be taken as the error in the normalization.	
	50H	Title	
2	ΔU_R Δr_{oR} Δa_R ΔW_S ΔW_D Δr_{oI} Δa_I ΔU_{so} ΔW_{so} Δr_{oc} $\Delta \beta$	Read only if I7=2, 7 or 8. These are the increments by which the (starting) values are changed after the completion of a run.	(13F5.4)
3	NUGV NRRGV NARGV NWSGV NWDGV NRIGV NAIGV NSPGV NWPGV	Card Set 3 must be read in if Card Set 2 is read in. These are the number of different parameter values that each calculation is to be started with.	(11I5)

TABLE A - 1 (Continued)

Card Set	Symbol	Definition	Format
	NRCGV		
	NBT		
4	E	Incident particle lab energy	(5F10.8)
	AM_T	Target Mass	
	AM_I	Incident particle mass	
	Z_T	Target charge	
	Z_I	Incident particle charge	
5	U_R	Real Potential Well Depth	(7F10.8)
	r_{oR}	Real Saxon well radius parameter	
	a_R	Real Saxon well diffuseness parameter	
	W_s	Imaginary Saxon well depth	
	W_D	Imaginary Saxon derivative well depth	
	r_{oI}	Imaginary Saxon radius parameter	
	a_I	Imaginary Saxon diffuseness parameter	
6	V_{so}	Real Potential Well Depth	(6F10.8)
	W_{so}	Imaginary Potential Well Depth	
	r_{os}	Potential radius parameter	
	a_s	Potential diffuseness parameter	
	β	Nonlocality range	
	r_{oc}	Coulomb radius parameter	
7	h_I	Integration step length (0.15)	(F10.8,F5.4, I5,4F10.8)
	α	Deuteron polarizability parameter	
	L_{max}	Max. number of partial waves	
	h_c	Coulomb integration step (0.1)	
	θ_{min}	Max. no. of angles = 100.	
	$\Delta\theta$		
	θ_{max}		
8	I1	= 1 (= 0) for spin (no spin) - orbit coupling	(5I1)
	I2	= 1 (= 0) to print (not print)	

TABLE A - 1 (Continued)

Card Set	Symbol	Definition	Format
		scattering coefficients, where $S_\ell = \exp(i\delta_\ell)$	
	I3	Redundant	
	I4	0, R_I independent of R_R; 1, $R_I=R_R$	
	I5	0, a_I independent of a_R; 1, $a_I=a_R$	
	I6	Redundant for single calculation. For search; 0, do not read in σ/σ_R. Plot of $\log_{10}(\sigma)$ versus θ c.m. 1, read σ/σ_R in column 31-40 of the first NS cards of card set 10. Plot of $\log_{10}(\sigma/\sigma_R)$ versus θ c.m. 2, read σ/σ_R in column 31-40 of the first NS cards of card set 10. Plot of both $\log_{10}(\sigma)$ versus θ c.m. and $\log_{10}(\sigma/\sigma_R)$ versus θ c.m.	
9	I_p (1-2)	= 0 print only final search = 1 print only χ^2 = 2 print χ^2 and angular distribution	(I2,F5.2, 2I2,2I1, 3I2,F14.9, 13I3)
	AKOFF(3-7)	Improvement in χ^2 to stop search	
	KM(8-9)	Max. no. of central guesses allowed, < 100	
	N(10-11)†	No. of variables being searched on	
	N_R(12)	= 1, σ_R searched on = 0, no search on σ_R	
	N_T(13)	= 1, σ_T search on = 0, no search on σ_T	
	N_S(14-15)	no. of points in $\sigma_{exp}(\theta)$	
	N_P(16-17)	no. of points in $P_{exp}(\theta)$	
	KR(18-19)	= 0, errors in σ, $P(\theta)$ are absolute = 1, $\Delta\sigma$, ΔP in % of $\sigma(\theta)$, $P(\theta)$	
	DELM(20-33)	Min. value of χ^2 satisfactory	
	IPA(I)(34-36)	Parameters being searched on	

†N = 0 gives a single calculation with a plot

TABLE A - 1 (Continued)

Card Set	Symbol	Definition	Format
10		In the current version of the program α and β cannot be searched upon. $\theta, \sigma(\theta), \Delta\sigma(\theta), \sigma(\theta)/\sigma_R(\theta)$ if I6=1,2 not if I6 = 0 $\theta, P(\theta), \Delta P(\theta)$ $\sigma_R, \Delta\sigma_R$ $\sigma_T, \Delta\sigma_T$ $N_S + N_P + N_R + N_T$ cards.	(4F10.8)

TABLE A - 2

I7	Function	Read Card Set 2,3 ?
0	Calls EXIT. This is the last data card.	-
2	Single calculation with subsequent grid variation of the parameters.	Yes
3	Single calculation with no grid variation.	No
4	Single search.	No
5	Search with same angles and cross section as in last set. Therefore omit card set 10.	No
6	Search with same data as in last set. Read in only card set 9.	No
7	Search with subsequent grid variation for starting values of the parameters.	Yes
8	As for I7 = 7 only same angles and cross sections as in last set. Therefore omit card set 10.	Yes

where $\underline{\ell}\cdot\underline{\sigma}$ is for spin 1/2 particles only and $f_{ws}(r,R,a) = 1/(1+\exp((r - r_o A^{1/3})/a))$. Table (A-2) contains the functions of I7. All lengths and energies are in fermis and MeV, respectively.

c. Comments on the Use of the Program

A six parameter search requires less than 10 minutes of computer time. It should be noted that a search with fewer free parameters can often yield a better fit as then there are fewer local minima in which the search can terminate. A need for renormalization of the experimental data is usually indicated by the preponderance of one sign in the values of chi.

Perey's program is about three times slower than the code Seek. The Vr^n ambiguity can best be treated by gridding over r_o and finding the minimum in the U-W-a space. In this respect the grid variation in the code SEEK is more sophisticated in that previous best fit values of the parameters are used in subsequent calculations. A complete set of data including polarization and reaction cross section as well as differential cross section generally removes such ambiguity.

The number of partial waves available in Perey's code was reduced from 50 to 40 [1] and the number of experimental points from 200 to 100 in order to calculate the Legendre polynomials only once. This and other modifications such as the elimination of unnecessary exponentiation to calculate form factors have speeded up the search by about 15%.

---

[1] 21.6 MeV deuterons on Mg^{24} require a maximum ℓ of 15.

REFERENCES

Aj 59 F. Ajzenberg-Selove and T. Lauritzen, Nucl. Phys. 11 (1959) 1

Al 60 W.D. Allen, Fast Neutron Physics (Interscience Publishers Inc., New York 1960) 3A, 361

Ba 57 S.J. Bame, E. Haddad, J.E. Perey, K.K. Smith, Rev. Sci. Inst. 28 (1957) 997

Ba 62 R.H. Bassel, Some Applications of the Distorted Wave Approximation for Direct Nuclear Reactions, ORNL-P-144 (1964)

Be 55 R.E. Benenson, K.W. Jones, M.T. McEllistrem, Phys. Rev. 101 (1956) 308

Bh 52 A.B. Bhatia, K. Huang, R. Huby, H.C. Newns, Phil. Mag. 43 (1952) 485

Bo 49 T.W. Bonner, J.E. Evans, J.C. Harris, G.C. Phillips, Phys. Rev. 75 (1949) 1401

Bo 56 T.W. Bonner, J.T. Eisinger, A.A. Kraus, J.B. Marion, Phys. Rev. 101 (1956) 209

Bu 60 B. Buck, R.N. Maddison and P.E. Hodgson, Phil. Mag. 5 (1960) 1181

Bu 61 B. Buck and P.E. Hodgson, Phil. Mag., 6 (1961) 1371

Bu 62 R. Butler and E. Kerr, An Introduction to Numerical Methods (Sir Isaac Pitman and Sons, Ltd., London, 1962) 6.2, 316

Bu 66 M.B. Burbank, M.Sc. Thesis, University of Alberta (1966) to be published

Ca 57 J.M. Calvert, A.A. Jaffe and E.E. Maslin, Proc. Phys. Soc. (London) A70 (1957) 78

Co 65 S. Cohen and D. Kurath, Nucl. Phys. 73 (1965) 1

Da 52 P.B. Daitch and J.B. French, Phys. Rev. 87 (1952) 900

Da 66 W.G. Davies, Ph.D. Thesis, University of Alberta (1966) unpublished

De 60 G. Dearnaley, Rev. Sci. Inst. 31 (1966) 197

Di 65 J.K. Dickens and F.G. Perey, Phys. Rev. 138 (1965) B1083

Dr 63 R.M. Drisko, G.R. Satchler, R.H. Bassel, Phys. Letters 5 (1963) 347

El 51 F.A. El-Bedewi, R. Middleton, C.T. Tai, Proc. Phys. Soc. (London) A64 (1951) 1055

El 59 A. Elwyn, J.V. Kane, S. Ofer, D.H. Wilkinson, Phys. Rev. 116 (1959) 1490

Ev 63 J.E. Evans, J.A. Kuehner, E. Almquist, Phys. Rev. 131 (1963) 1632

Fo 49 L. Fox and E.T. Goodwin, Proc. Cambridge Phil. Soc. 45 (1949) 373

Fr 60 J.B. French, Nuclear Spectroscopy (Academic Press, New York, 1960) V-G, 890

Fu 66 H.W. Fulbright, J.A. Robbins, R. West, Nucl. Phys. (to be published)

Ge 66 D.A. Gedcke, Modifications to TMC Analyzers, University of Alberta internal report (1966)

Gi 61 W.R. Gibbs and W. Tobocman, Phys. Rev. 124 (1961) 1496

Gl 63 N.K. Glendenning, Annual Review of Nuclear Science, 13 (1963) 191

Go 61 H.E. Gove, A.E. Litherland, R. Batchelor, Nucl. Phys. 26 (1961) 480

Gr 49 J.C. Grosskreutz, Phys. Rev. 76 (1949) 482

Gr 65 T.B. Grandy, Relativistic Kinematics, University of Alberta internal report (1966)

Ho 61 T. Honda and H. Ui, Prog. Th. Phys., 25 (1961) 635

Ho 63 P.E. Hodgson, Proc. Phys. Soc. 81 (1963) 977

Ho 63a P.E. Hodgson, The Optical Model of Elastic Scattering (Oxford University Press, London, 1963) 6.1, 119

Ja 51 H.L. Jackson and A.I. Galonsky, Phys. Rev. 83 (1951) 876

Ja 61 A.N. James, Nucl. Phys. 23 (1961) 648

Je 63 J.M.F. Jeronymo, G.S. Mani, F. Picard, A. Sadeghi, Nucl. Phys. 43 (1963) 417

Ko 63 N. Kolonko, A. Lewandowski, M. Makowska-Rzeszutko, H Niewodniczański, S. Wiktor, Z. Wróbel, Acta Phys. Polon. 23 (1963) 225

La 53 A.M. Lane, Proc. Phys. Soc. A66 (1953) 977, A67 (1954) 167, A68 (1955) 197

Le 63 L.L. Lee, Jr. and J.P. Schiffer, Phys. Rev. 136 (1964) B405

Lu 57 C.R. Lubitz, Numerical Table of Butler-Born Approximation Stripping Cross Sections, University of Michigan, unpublished

Ma 60 M.H. MacFarlane and J.B. French, Rev. Mod. Phys. 32 (1960) 567

Ma 62 R.N. Maddison, Proc. Phys. Soc., 79B (1962) 264

Ma 66 R.N. Maddison, J.A.C.M., 13 (1966) 124

Mc 58 M.T. McEllistrem, Phys. Rev. 111 (1958) 596

Me 64 A. Messiah, Quantum Mechanics (North-Holland Publishing Company, Amsterdam, 1964) X, 405

Me 65 M.A. Melkanoff, T. Sawada and J. Raynal, Nuclear Optical Model Calculations, to be published in Vol. V of Methods in Computational Physics (Academic Press, New York, 1966)

Me 66 M.A. Melkanoff, T. Sawada, J. Raynal, SEEK, Report No. 66-10, UCLA (1966)

Mi 53 R. Middleton, F.A. El-Bedewi and C.T. Tai, Proc. Phys. Soc. (London) A66 (1953) 95

Mo 65 N.F. Mott and H.S.W. Massey, The Theory of Atomic Collisions (Oxford University Press, London, 1965) XX, 6.2, 754

Nu 65 Nuclear Enterprises Ltd., Winnipeg, Canada, Scintillator Catalogue (1965)

Pe 63 C.M. Perey and F.G. Perey, Phys. Rev. 132 (1963) 755

Re 66 W.B. Reid and R.H. Hummel, Can. Nucl. Tech., Jan.-Feb. (1966) 36

Ro 51 J. Rotblat, Phys. Rev. 83 (1951) 1271

Sc 63 U. Schmidt-Rohr, R. Stock, P. Turek, Nucl. Phys. 53 (1964) 77

Sh 62 I.S. Shapiro, Uspekhi 4 (1962) 674

Sm 63 W.R. Smith and E.V. Ivash, Phys. Rev. 131 (1963) 304

Sm 65 W.R. Smith, DWB Deuteron Stripping Program, ORNL-TM-1151

Sw 60 C.D. Swartz and G.E. Owen, Fast Neutron Physics (Interscience Publishers Inc., New York, 1960) II B, 211

Te 66 J.W. Tepel, Nucl. Inst. Meth. 40 (1966) 100

Va 49 D.M. Van Patter, Phys. Rev. 76 (1949) 1264

Wi 55 D.H. Wilkinson, Phys. Rev. 100 (1955) 32

Wi 58 D.H. Wilkinson, Phil. Mag. 3, (1958) 1185

Wi 63 D.L. Wieber, Nucl. Inst. and Meth., 24 (1963) 269

Wi 66 D.G. Gerke, D.R. Tilley, N.R. Fletcher and R.M. Williamson, Nucl. Phys. 75 (1966) 609